The Function of Coordinated Neuronal Ensembles in the Auditory Thalamocortical System

by
Congcong Hu

DISSERTATION
Submitted in partial satisfaction of the requirements for degree of
DOCTOR OF PHILOSOPHY

in

Neuroscience

in the

GRADUATE DIVISION
of the
UNIVERSITY OF CALIFORNIA, SAN FRANCISCO

Approved:

Vikaas Sohal
                                                                    Chair

Christoph Schreiner

Christoph Kirst

Michael Brainard

                                                        Committee Members

Acknowledgments

I would like to thank my thesis committee members: Vikaas Sohal, Micheal Brainard, Christoph Kirst, and Christoph Schreiner, for their invaluable support throughout this entire project. A special thank you is extended to my thesis advisor, Dr. Christoph Schreiner, for his unwavering intellectual guidance during the course of this thesis work. His mentorship consistently illuminated my path when I found myself in need of direction.

I have been fortunate to work with exceptional individuals in the Coleman lab, who have not only been great friends but also invaluable collaborators. I must express my sincere gratitude to all of them. In particular, I am deeply appreciative of Dr. Homma Natsumi for her overwhelming support, which has transformed my graduate training into a profoundly memorable and enjoyable experience.

Furthermore, I wish to acknowledge the support of the neuroscience graduate program at UCSF. My special thanks go to the program administrators, Pat Veitch and Lucita Nacionales, whose efforts have ensured that my journey through the program was smooth and rewarding.

Finally, I want to express my gratitude to my family and friends, both near and far, for their unwavering support that has kept me grounded over the years. I want to thank my partner, William, for his constant companionship, comfort, and encouragement throughout this entire experience.

The Function of Coordinated Neuronal Ensembles in the Auditory Thalamocortical System

Congcong Hu

Abstract

Coordinated neuronal activity plays an important role in information processing and transmission in the brain. With current research predominantly focuses on understanding the properties and functions of neuronal coordination within cortical areas, however, whether coordinated neuronal ensembles (cNEs) are unique to cortical local networks or extend to neuronal populations in other brain regions, such as the auditory thalamus, remains unknown. Additionally, questions persist regarding whether information carried by cNEs is effectively transmitted to downstream areas compared to single neurons. In this study, we use single-unit recordings in female Sprague-Dawley rats to investigate the properties and functions of groups of neurons exhibiting coordinated activity in the auditory thalamus – the medial geniculate body (MGB). We reliably identify cNEs, which are groups of neurons that fire synchronously, in the MGB. We demonstrate that cNEs in the MGB have enhanced information encoding properties and are stable between spontaneous and evoked activity. These MGB cNE properties are similar to what is observed in the cNEs in the primary auditory cortex (A1), suggesting that ensembles serve as a ubiquitous mechanism for organizing local networks, playing a fundamental role in sensory processing within the brain. Furthermore, spikes from MGB neurons synchronized with other cNE members exhibit higher efficacy in driving A1 neuron firing compared to spikes unrelated to cNE activities. This increased efficacy of cNE spikes is target-specific and cell-type specific, rather than resulting in a general increase in the firing rate across all A1 neurons. These findings support the concept of a neuronal ensemble as a functional unit for encoding and transmitting information in the forebrain processing.

iv

Table of Contents

List of Figures

List of Abbreviations

A1   primary auditory cortex

BS   broad-spiking

BF   best frequency

CCG   cross-correlogram

CF   characteristic frequency

cNEs   coordinated neuronal ensembles

CV   coefficient of variation

DMR   dynamic moving ripple

FR   firing rate

IC   independent component

ICA   independent component analysis

ISI   inter-spike interval

LGN   lateral geniculate nucleus

MGB   medial geniculate body

MI   mutual information

MU   multi-unit

NS   narrow-spiking

PC   principal component

PCA   principal component analysis

PTD   peak-trough difference

SD   standard deviation

SNR   signal-to-noise ratio

STRF   spectrotemporal receptive fields

SU   single unit

TPD   trough-to-peak duration

Introduction

The question of how neurons encode and transmit information has long been a central focus in systems neuroscience. Early studies concentrated on unraveling the firing patterns of individual neurons, yet an evolving body of evidence, particularly from investigations into neuronal correlations, underscores the pivotal role of the temporal relationship of spikes fired by multiple neurons. An analysis of pairs of visual neurons in the lateral geniculate nucleus (LGN) revealed that when synchronous spikes are considered separately from non-synchronous ones, significantly more information about visual stimulus can be extracted (Alonso et al., 1996). Recordings in A1 also showed that continuous sounds can induce sustained increases in pairwise correlations between neurons while firing rate modulation of individual neurons is only transient upon sound arrival (Decharms and Merzenich, 1996). These findings underscored the encoding potential of temporal coordination of neural activities, complementing the information derived from the firing rate modulation of individual neurons.

While studies focusing on pairwise correlations have demonstrated the encoding potential of neuronal pairs, it has become evident that such correlations might not sufficiently describe the role neuronal coordination plays in certain behavioral conditions. A study in the visual cortex showed that precise temporal coordination of more than two neurons carries information about the task performance of the animal, but such information cannot be extracted from pairwise correlation (Shahidi et al., 2019). In the context of coordinated activities in A1 columns, the identification of cNEs with multiple neuron members through dimensionality-reduction techniques (Lopes-dos Santos et al., 2013) led to the discovery that cNEs represent functionally stable and connected local network configurations (See et al., 2018). Remarkably, cNE events were found to convey more information about auditory stimuli than the spikes of individual member neurons. As single neurons can encode multiple signals (Lankarany et al., 2019), the enhanced information value of cNE events suggests a reduction in noise, isolating specific signals

from a mixed pool. This leads us to propose that cNEs serve as physiological units for auditory information encoding and transmission.

To validate cNE activities as viable neural codes, it is imperative to identify a biological implementation capable of propagating cNE activities to downstream brain regions. It was suggested that temporal coordination, which is the nature of cNE activity, in a source population can increase the efficacy of neural signaling (Zandvakili and Kohn, 2015). This was supported by evidence from the physiological properties of neurons, which make them sensitive to the timing of synaptic inputs (Alonso et al., 1996; Usrey et al., 2000). Neuronal spiking typically results from the integration of a range of spatiotemporally distributed synaptic inputs. The effectiveness of a spike can be influenced by its temporal relationship with spikes fired by another neuron connected to the same target (Usrey et al., 2000). While earlier studies provided valuable insights into how coordination influences the spiking of target neurons (Usrey et al., 2000; Zandvakili and Kohn, 2015), these investigations primarily focused on pairwise correlation and did not explore higher-order coordination captured by cNE activities. Thus, it remains unclear how higher-order coordination, as captured by cNE activities in a source population, influences their ability to induce firing in target cells and how response properties of target cells are shaped by the coordinated inputs.

In this study, we employ a combined analysis of coordinated activities among groups of neurons and the response features of individual neurons to elucidate the functional consequences of neuronal coordination. We conducted simultaneous recordings of neural activities from the auditory thalamus (the medial geniculate body, MGB) and the A1. We consistently identified cNEs in the MGB, representing groups of neurons exhibiting correlated firings. Shared key characteristics were observed between cNEs in the MGB and A1, with both structures displaying highly similar cNEs in spontaneous and stimulus-driven activities. Additionally, spikes associated with cNEs ("cNE spikes") were found to offer a more reliable reflection of auditory information compared to random spikes from the same neurons. Notably, cNE spikes from MGB neurons

demonstrated higher efficacy in driving A1 neuron firing than spikes unrelated to cNE activities ("non-cNE spikes"). This increased efficacy of cNE spikes was exclusively observed in cases where the A1 target neuron was narrow-spiking (NS), with no such effect observed in broad-spiking (BS) A1 neurons. Furthermore, the heightened efficacy of cNE spikes was target-specific, rather than resulting in a general increase in the firing rate across all A1 neurons. These findings support that neurons cooperate in units of cNE to encode and transmit information in the brain.

Chapter 1: Basic Properties of Neuronal Ensembles in the Auditory Thalamus

1.1 Introduction

The function of coordinated neuronal activity in cognitive processes has long been a subject of interest in systems neuroscience (Konorski, 1948; Hebb, 1949). Initially, such activity was difficult to observe experimentally. However, recent technological advancements in large-scale recording, such as two-photon imaging and high-density multi-channel probes, have facilitated extensive investigations into the properties and functions of coordinated neuronal firing, primarily within the hippocampus and neocortex (Laubach et al., 2000; Baeg et al., 2003; Harris et al., 2003; Bizley et al., 2010; Buzsáki, 2010; Bathellier et al., 2012; Oberto et al., 2022; Boucly et al., 2022; Domanski et al., 2023). These studies have revealed temporal coordination among neurons in several brain areas, shedding light on their potential roles in various cognitive processes, such as perception, memory formation, and decision making. Indeed, neuronal ensembles have been proposed as the fundamental units for information processing and transmission (Buzsáki, 2010; Yuste, 2015).

In sensory systems in particular, temporal coordination among neurons has been proposed as a mechanism to enhance information processing citepkreiter1996stimulus, dan1998coding, See2018, See2021 and facilitate communication within and between brain regions (Zandvakili and Kohn, 2015; Oberto et al., 2022). Neuronal coordination allows more reliable and specific representation of stimuli (See et al., 2018; Yoshida and Ohki, 2020; See et al., 2021; Ebrahimi et al., 2022), and considering neuronal coordination allows identification of emergent stimulus encoding properties (Decharms and Merzenich, 1996; Shahidi et al., 2019). Additionally, elevated coordination in neuronal activity in an output or sender area often precedes activity in a target or receiver area (Zandvakili and Kohn, 2015). Thus, it is crucial to investigate the expression of cNE structure and function at various stages along the sensory pathway.

In the auditory system, A1 contains pairs of neurons with correlated activity (Brosch and Schreiner, 1999; Eggermont, 2000; Atencio and Schreiner, 2013) as well as larger groups of neurons with correlated firing. These groups contribute to the representation of auditory stimuli (Kreiter and Singer, 1996; Miller and Recanzone, 2009; Ince et al., 2013; See et al., 2018). While characteristics of coordinated activity within the cortex have recently been studied (Bathellier et al., 2012; Chamberland et al., 2017; See et al., 2018, 2021), our understanding of the organization and functional significance of neuronal ensembles in subcortical regions, such as the thalamus, remain unknown. The thalamus is of particular interest since it is the gateway and a direct intermediary between the peripheral sensory system and the cortex (Winer et al., 2005; Smith et al., 2012; Bartlett, 2013). The auditory thalamus MGB and A1 are highly interconnected, with structured connections linking neurons which share similar spectral and temporal response properties (Miller et al., 2002; Bartlett and Wang, 2007). Considering the strong connections between the thalamus and cortex, investigating the shared characteristics of neuronal ensembles in both regions will help us better understand the role these ensembles may play in auditory information processing and transmission, and sensory processing in general.

In this study, we aimed to identify and characterize coordinated neuronal ensembles (cNEs) in the MGB. We reliably detected cNEs, defined as groups of neurons exhibiting temporally highly coordinated activity, in the MGB. The applied detection method showed robustness, consistently identifying cNEs across different time bin sizes. Importantly, we observed a high degree of similarity between cNEs derived from spontaneous and evoked activity, suggesting that these ensembles represent functional networks that can operate, to a substantial degree, independently of specific sensory stimuli. Furthermore, cNEs in the MGB and A1 shared key characteristics. In both structures, spikes associated with cNEs reflect auditory information more reliably than random spikes from the same neurons. These findings support the hypothesis that cNEs serve as a ubiquitous mechanism for organizing local networks and function as fundamental units for sensory processing in the brain.

1.2 Results

Auditory responses in MGB

We conducted extracellular recordings in the rat MGB (Figure 1.1A) using a 64-channel linear probe, which allowed us to cover most of its span along the dorsal-ventral axis. To obtain the tonal response properties of the recording sites, we presented pure tones of various frequencies and intensities. In the MGB, we usually observed a gradient in the frequency preference of multi-unit (MU) responses from low to high along the dorsal-ventral axis, which could vary gradually (Figure 1.1A-i) or abruptly (Figure 1A-ii) depending on the probe's location. Responses on most channels in the tonotopic region exhibited clear frequency tuning (between the red lines in Figure 1.1A), which likely reflect activities in the ventral MGB, the primary input station to the A1. We included all single units (SUs) from the MGB in our analysis after spike sorting, without distinguishing between sub-regions although the vast majority was likely from the ventral nucleus according to its tonotopic organization.

To estimate the spectrotemporal receptive fields (STRF) of SUs, we used a 15-minute dynamic moving ripple (DMR) stimulus, which is a broadband noise with varying spectral and temporal modulation (Escabí and Schreiner, 2002). The STRFs of MGB neurons also showed a clear gradient in frequency preference from low to high along the dorsal-ventral axis (Figure 1.1B), consistent with the MU responses to pure tones. We then examined the firing correlations between pairs of simultaneously recorded SUs. MGB neuron pairs showed widely different correlations in their firing activity, even if they were close in proximity and had similar STRFs. For example, Neurons #1, #2, and #3 had similar receptive fields (Figure 1.1B). While neurons #1 and #3 showed correlated firing in both stimulus-driven and spontaneous activity, neurons #2 and #3 showed no significant correlation in their activity despite similar STRFs (Figure 1.1C). This diversity of correlation patterns, even among neurons with similar receptive fields, parallels what was previously observed in the cortex (Brosch and Schreiner, 1999; Eggermont, 2000; Atencio and Schreiner, 2013; See et al., 2018; Mogensen et al., 2019; Wahlbom et al., 2021). Although

the role of neuronal coordination in information processing in the cortex has been extensively proposed and studied (Paninski et al., 2004; Bizley et al., 2010; Buzsáki, 2010; Carrillo-Reid et al., 2015; See et al., 2018), less is known about the organization of neuronal ensembles in subcortical regions. Therefore, we aimed to identify clusters of neurons that exhibit consistent synchronized firing in the MGB and compared the properties of these ensembles with those in A1.

Identifying groups of neurons with coordinated firing in MGB

To identify cNEs, i.e., groups of neurons with synchronous firing, we performed a combined principal- and independent-component analysis (PCA-ICA) (Lopes-dos Santos et al., 2013; See et al., 2018). The procedure for detecting cNEs in a population of neurons is demonstrated in Figure 1.2A using a recording of spontaneous activity from the MGB (Figure 1.2A). Among the 20 isolated single units in the recording, some pairs of neurons had highly correlated firing with each other, as shown in dark red in the correlation matrix, while others showed low correlation (Figure 1.2A-i). We performed PCA on the correlation matrix of 10ms-binned spike trains, resulting in 20 eigenvalues and corresponding eigenvectors or principal components (PCs) (Figure 1.2A-ii). These eigenvalues describe the contribution of each PC to the variance in the neural population activity. To determine the significance of the patterns extracted by PCA, we compared the eigenvalues to a threshold drawn based on the Marchenko-Pastur distribution (Peyrache et al., 2010; Lopes-dos Santos et al., 2013) (Figure 1.2A-ii). In this example recording, we observed four significant eigenvalues above the threshold, indicating the presence of four detectable cNEs in the recorded population. Although PCA efficiently extracts ensemble patterns, it has some limitations due to its variance maximization framework. When two ensembles account for similar variance in the data on their corresponding axis, the first PC will represent the average of the two instead of an individual ensemble. This problem is even more pronounced when ensembles share neurons. To overcome these limitations, we applied ICA to the subspace spanned by the significant PCs (Figure 1.2A-iii). This approach is not constrained by the orthogonality requirement of PCA, allowing for a more precise identification of individual cNEs. After the PCA-ICA procedure, we obtained the weights of neurons on the axes that define cNEs in the

7

neural population, which were color-coded as columns in Figure 1.2A-iii. Neurons were considered members of a cNE if their independent component (IC) weights were higher than what would be expected from an even weight contribution from all neurons (Figure 1.2A-iv). The activity resulting from co-activation of cNE members can be obtained by projecting the spike matrix on the corresponding IC weights of the cNE. To determine the significance of cNE activity magnitude, we generated a null distribution of the cNE activity values by circularly shuffling spike trains and set the significance criteria at 99.5% (Figure 1.2A-v). For example, when cNE #1 was active, multiple member neurons (2-5 out of 6) fired together. The combined PCA-ICA approach provided a useful framework to investigate the organization and function of coordinated neuronal activity in the MGB.

To provide evidence that cNEs captured groups of neurons with correlated firing, we compared the correlations of 10ms-binned spike trains based on their cNE membership. Pairs of neurons that participated in the same cNE ("member pairs") exhibited significantly higher correlations compared to pairs of neurons that did not share membership in any cNE ("non-member pairs") (Figure 1.2B). To examine the correlation between member and non-member pairs at a finer timescale, we cross-correlated the spike trains using 1ms bins. The correlation among cNE member pairs was significantly higher compared to non-member pairs within the [-50, 40] ms lag window (red-shaded area in Figure 1.2C, bottom left). These results provided evidence that groups of neurons with coordinated firing exist in the MGB, and that their coordination was captured by the PCA-ICA procedure, resulting in the identification of cNEs.

Variability in cNE identity for different bin sizes

The temporal frame used to identify neuronal ensembles plays a critical role in shaping our understanding of their nature and function (Buzsáki, 2010). To investigate how different choices of timescale affect the identification of cNEs, we calculated cNEs using various spike train bin sizes, ranging from 2ms to 160ms (Figure 1.3). Some cNEs showed consistent IC weights across different time bin sizes, with a high correlation to IC weights obtained using 10ms bins (Figure

1.3A-i). Other cNEs could only be consistently identified using smaller time bin sizes but deviated from those when assessed with larger bin sizes (Figure 1.3A-ii). We matched cNEs calculated using different bin sizes to evaluate their similarity (Figure 1.3B). With only small change in the bin size, the cNEs identified were highly similar. For example, 96% of cNEs identified using 10ms bins had a significant match with 20ms cNEs. However, when compared to cNEs calculated with larger differences in bin sizes, their identities could vary substantially. For example, 43% of 10ms cNEs did not show a significant match with 160ms cNEs (Figure 1.3B). The remaining 57% of 10ms cNEs that significantly matched 160ms cNEs exhibited high correlation (>0.6) in their IC weights (Figure 1.3C-i). Moreover, the majority of significantly matched cNEs shared more than half of their neuron membership. Nonetheless, approximately 25% of 10ms cNEs had no common members with the 160ms cNEs (Figure 1.3C-ii). There was no significant difference in the firing rate of MGB neurons participating in 10ms and 160ms cNEs (Figure 1.3D). In summary, small variations in time bin sizes have a limited effect on cNE identity. However, using large time bin sizes to identify cNEs, such as 160ms, may result in the loss of half or more of the cNEs identified using small bin sizes, such as 10-20ms.

In cases where differences in cNE membership arise due to different bin sizes, we investigated the firing correlations between neurons that had shifted in or out of the ensemble. We compared the membership of neurons in cNEs identified using 10ms and 160ms bin sizes ("10ms cNEs" and "160ms cNEs", Figure 1.3E) and categorized neurons in each cNE as the following: members in both 10ms and 160ms cNEs, members only in the 10ms cNE, or members only in the 160ms cNE. Neurons sharing memberships in both 10ms and 160ms cNEs (stable members) had positive correlations in their firing (Figure 1.3E-i). Neurons only in 160ms cNEs were positively correlated with stable members, although the correlation was significantly weaker in the [-17, 10] ms window (Figure 1.3E-ii) compared to the correlation among stable members (Figure 1.3E-i). Furthermore, some members of 10ms cNEs were not identified as members in 160ms cNEs. These neurons showed no significant difference in their correlations with stable members (Figure 1.3E-iii) compared to the correlation among stable members (Figure 1.3E-i). Therefore, using

9

wider bin sizes to identify cNEs results in neurons with weak correlations being included in the ensemble, as well as neurons with strong correlations being omitted.

Variability in cNE structures across spontaneous and evoked activity

Several studies have shown that cortical neuronal ensembles have stable structures across spontaneous and stimulus-driven activity, suggesting a consistent local network organization utilized in processing stimulus information (Jermakowicz et al., 2009; Luczak et al., 2009; See et al., 2018; Filipchuk et al., 2022). To investigate if this property also exists in cNEs in the MGB, as was observed in A1 (See et al., 2018), we recorded continuous segments of neural activity in the absence of sound (spontaneous, hereafter 'spon') and during the presentation of the DMR stimulus ('dmr'). We divided each activity type into two segments and detected cNEs in each segment separately. We then compared the stability of the cNEs within and across stimulus conditions, measured by the correlation of IC weights between adjacent segments (Figure 1.4A and B). We observed that while some cNEs exhibited high stability across stimulus conditions, with IC weights correlation comparable to that within the same stimulus condition (Figure 1.4C-i), others showed structures that were less stable across stimulus conditions compared to within a stimulus condition (Figure 1.4C-ii). Using null distributions generated by circularly shuffling spikes, we determined the significance of the IC weight correlations and found that both examples in Figure 1.4C were significantly stable across stimulus conditions, although one was slightly more stable than the other (Figure 1.4D). In MGB, within spontaneous or stimulus-driven activity, around 80% of cNEs exhibited stable structures across adjacent activity blocks (Figure 1.4E). Significantly fewer cNEs (54.8%) were stable across stimulus conditions than within a stimulus condition (spon vs cross, p = 0e-4; dmr vs cross, p = 6e-4; spon vs dmr, p = 1.0, permutation test with Bonferroni correction). The results provide evidence for the stability of cNEs in the MGB, during both spontaneous and stimulus-driven activity, although fewer cNEs exhibit stable structures across different stimulus conditions than within the same stimulus condition.

To test the possibility of false positive detection of cNEs, we generated shuffled data on each segment by circularly shifting spike trains to disrupt their temporal correlations. We then applied the cNE detection algorithm to the shuffled data using the same criteria as for the real data. Our analysis revealed a drastically lower number of cNEs identified in shuffled segments (real data vs. shuffled data, spon1: 3.2 ± 0.9 vs 0.2 ± 0.3; spon2: 3.1 ± 0.7 vs 0.3 ± 0.4; dmr1: 3.1 ± 0.9 vs 0.1 ± 0.2; dmr2: 3.2 ± 1.1 vs 0.1 ± 0.1, mean $\pm$ standard deviation (SD)) (Figure 1.4F), suggesting that the chance of false positive detection of cNEs is quite low. Furthermore, any cNEs identified in the shuffled data did not exhibit the same stability across stimulus conditions observed in real data (Figure 1.4E). In summary, our findings indicate that the detection of cNEs in the MGB is reliable and not susceptible to false positives. Moreover, the properties of cNEs we observe, such as their stability across stimulus conditions, are genuine and not artifacts of random data.

cNE properties in MGB

We determined some basic structural properties of MGB cNEs. The spontaneous activity in 34 MGB recordings revealed 115 cNEs with 3.4 ± 0.9 cNEs per penetration. More cNEs were observed in penetrations that captured a higher number of isolated single units (Figure 1.5A). The mean cNE size was 4.3 ± 1.5 members, dependent on the number of isolated neurons (Figure 1.5B). Of the 407 neurons isolated in MGB, the majority (78.6%) belonged to a single cNE, 11.5% did not belong to any cNE, and 9.8% belonged to multiple cNEs (Figure 1.5C).

Next, we investigated whether cNE members were physically and functionally closer to each other than non-member pairs of neurons. The pairwise spatial distance of cNE members was significantly smaller than that of non-member pairs of neurons in MGB (Figure 1.5D-i). Moreover, the span of cNEs, defined as the longest pairwise distance among all members, was shorter than that of randomly selected groups of neurons in the recording (Figure 1.5D-ii). The tuning of cNE members was also closer to each other, as the difference in the best frequency (BF) between cNE member pairs was smaller than that of non-member pairs (Figure 1.5E-i). The BF span of cNEs, defined as the largest difference in BF among all members, was smaller than that of

11

randomly selected groups of neurons (Figure 1.5E-ii). Our results demonstrate that cNEs in the MGB are composed of neurons that are physically and functionally closer to each other than non-member pairs, suggesting a pattern of local circuit organization as well as local functional congruence.

cNEs enhance stimulus information encoding

Synchronization of neuronal spikes in the cortex has been found to enhance information encoding about a stimulus compared to the participating neurons alone (Dan et al., 1998; Atencio and Schreiner, 2013; See et al., 2018). This is consistent with the multiplexed nature of an individual spike train, whereby spikes representing distinct stimulus aspects are mixed but can be separated based on their synchrony with other neurons (Lankarany et al., 2019; See et al., 2021). To investigate whether spikes from individual neurons that participate in cNEs also exhibit differential coding compared to the neuron's entire spike train, we compared the STRFs calculated using all the spikes emitted by a neuron to STRFs only based on the subset of spikes that contributed to cNE events ('cNE spikes'; Figure 1.6A). The spike trains were subsampled to ensure an equal number of spikes across conditions. Our analysis revealed that the STRFs of cNE spikes exhibit stronger excitatory and inhibitory fields compared to the STRFs of all spikes from the same neuron, as evidenced by the larger peak-trough difference (PTD) of the cNE STRFs (Figure 1.6B-i), which quantifies the difference between the largest and smallest value in the STRF. Given that PTD only considers two extreme values in the STRF, we further evaluated the reliability of cNE spikes relative to all spikes in encoding the sound features represented by their STRFs by calculating the mutual information (MI) between the stimulus and the spikes. Our results demonstrate that cNE-spike STRFs have higher MI than STRFs constructed from all spikes (Figure 1.6C-i).

To demonstrate that the increased information conveyed by cNE spike STRFs was not simply because cNEs integrate signals over multiple neurons, thus must enhanced information through population encoding, we compared STRFs derived from cNE member and non-member neurons.

First, we compared the multi-unit STRFs of cNE member neurons (cNE group STRF) with those of a neuronal group devoid of neurons sharing membership from any cNE (non-cNE group STRF). The cNE group STRFs exhibited a significantly higher MI than that of the non-cNE STRFs, although no significant difference in PTD was observed (Figure 1.6B-ii and C-ii). As the group STRFs did not take spike synchrony into account, we further compared cNE spikes and coincident spikes of a cNE member. The coincident spikes refer to spikes that occurred within a 10ms window relative to firing of other neurons not sharing membership with the neuron under examination. Both the PTD and MI of cNE spike STRFs were significantly higher than that of the coincident spike STRFs (Figure 1.6B-iii and C-iii).

Collectively, these findings suggest that cNE spikes can enhance information processing by increasing the signal-to-noise ratio and promoting more consistent encoding of certain stimulus features compared to including all spikes from the neuron. Furthermore, the enhanced information encoding of cNEs is not a trivial result of population encoding but rather hinges on the identity of cNE members and synchronous spike events.

MGB and A1 cNEs have similar properties

The properties and functions of cNEs have previously been explored within A1 (See et al., 2018, 2021), whereas investigations into cNEs in subcortical regions are limited. Hence, we aim to determine whether the properties of cNEs in the MGB differ substantially from those observed in A1 cNEs, or if they share similarities. To target A1, we used a 2-shank probe with 64 channels. The MU responses to pure tones from the two shanks of the probe exhibited similar frequency tuning, as the shanks sampled nearby cortical columns (Figure 1.7A). The responses on each shank showed small variation in their frequency preference along the depth of the probe, as neurons in the same cortical column have consistent characteristic frequencies across the active middle and deep cortical layers (Atencio and Schreiner, 2010; Merzenich et al., 1975). Much like cNEs in MGB, cNE spike STRFs in A1 exhibited higher PTD and MI compared to all spike STRFs (Figure 1.7B-i and C-i). Compared to A1 neurons, MGB neurons displayed significantly higher STRF PTD (all

spike STRF PTD, p = 3.1e-42; cNE spike STRF PTD, p = 8.6e-36) and mutual information (all spike STRF MI, p = 1.9e-25; cNE spike STRF MI, p = 4.2e-22). We did not observe, however, a significant difference between MGB and A1 cNEs regarding their gain in cNE spike STRF PTD and MI values over that of member neuron spiking (Figure 1.7B-ii and C-ii).

Addressing concerns of potential false positive detection in A1, we compared the number of cNEs detected on real and shuffled activities. A substantially smaller number of cNEs were detected on shuffled data compared to real data (real data vs. shuffled data, spon1: 4.6 ± 1.5 vs 0.9 ± 0.6; spon2: 4.2 ± 1.2 vs 1.1 ± 0.6, dmr1: 4.3 ± 1.5 vs 0.9 ± 0.6, dmr2: 4.2 ± 1.2 vs 1.0 ± 0.8, mean $\pm$ SD) (Figure 1.7D). Moreover, A1 cNEs were mostly stable across stimulus conditions, similar to MGB cNEs, whereas false positive cNEs did not show such stability (Figure 1.7E). The similarity between MGB and A1 cNEs in their stability across stimulus conditions and enhanced information encoding provides support for the concept of cNEs serving as a universal mechanism for neuronal organization and information processing.

cNE formation does not rely on strong slow oscillations

Slow-wave oscillations, characterized by alternating periods of large and sustained network activity (UP states) and neural quiescence (DOWN states), are frequently observed in the cortex and thalamus during anesthesia (Steriade et al., 1993; Contreras et al., 1996; Sanchez-Vives and McCormick, 2000; Hasenstaub et al., 2007; Chauvette et al., 2011; Neske, 2016). To quantify the level of slow oscillations in the recording and their potential influence on cNE properties, we used two measurements: silence density and the coefficient of variation (CV) of the MU firing rate. Silence density represents the proportion of recording time when no spike was fired by the neural population, which is characteristic of the DOWN state in slow oscillations. In brains without strong slow oscillations, the population of neurons fires continuously, resulting in low silence density. The MU firing rate CV measures the level of variation in the firing rate of the MU, which is high for neurons going through UP-DOWN state cycles, but small for neural populations with less synchronized oscillatory activity. Recordings with high silence density and high MU firing

14

rate CV showed prominent slow oscillations, with epochs of synchronous firing of neurons and epochs of quiescence with no spikes (Figure 1.8A-i). In contrast, recordings with low silence density and low MU firing rate CV did not exhibit strong slow oscillations, displaying relatively stable and continuous firing (Figure 1.8A-ii). Recordings with moderate silence density and MU firing rate CV exhibited moments of elevated firing, although not as synchronized as in recordings with strong oscillations (Figure 1.8A-iii). By utilizing silence density and MU firing rate CV, we were able to differentiate recordings without strong slow oscillations from those with strong slow oscillations.

The relationship between cNEs and slow oscillations was investigated by applying the cNE detection algorithm to recordings without strong oscillations in response to DMR during 15-minute recordings. Recordings exhibiting low silence density and low CV of the MU firing rate were selected to ensure the absence of strong slow oscillations (n(animals): MGB = 8, A1 = 18; n(recordings): MGB = 13, A1 = 10). To determine whether cNEs were solely a byproduct of slow oscillations, we compared the number of cNEs detected in these recordings against the expected false positive rate. We found a significantly higher occurrence of cNEs in activity characterized by low silence density and low MU firing rate CV in both MGB (n(cNE) = 3.9 $\pm$ 1.0, mean $\pm$ SD; p = 2.4e-4, Wilcoxon signed-rank test) and A1 (n(cNE) = 5.2 $\pm$ 1.9, p = 0.002) when compared to shuffled data (as in Figure 1.5). This supports the notion that cNEs are not a byproduct of slow oscillations.

Slow oscillations in thalamic and cortical firing rates are commonly observed and can be related to synchronized and desynchronized states of the system (Metherate and Ashe, 1993; Steriade et al., 1993; Cowan and Wilson, 1994; Sanchez-Vives and McCormick, 2000; Hasenstaub et al., 2007). However, the effect of firing rate changes on the information carried by cNEs is not known. Therefore, we tested whether cNE spikes exhibit enhanced information encoding in recordings without strong oscillations in response to the stimulus. The results showed that cNE spike STRFs have higher MI compared to all spikes in both MGB and A1 (Figure 1.8B), indicating that enhanced

information encoding is not specific to synchronized states under slow oscillations. Additionally, a subset of recordings did not show strong slow oscillations in either stimulus-driven or spontaneous activity (n(animals): MGB = 4, A1 = 6; n(recordings): MGB = 5, A1 = 8). We also examined the stability of cNEs across and within stimulus conditions in these recordings. The majority of cNEs were stable both within and across stimulus conditions (Figure 1.8C). In summary, cNEs exist in both MGB and A1 without the presence of strong slow oscillations in neural activity. Their enhanced information encoding and stability across stimulus conditions are not due to a special behavior of neurons in synchronized states under slow oscillations.

Synchrony-based cNEs are distinct from rate-based neuronal groups

Previous studies have proposed a manifestation of ensemble coding based on neuronal groups with co-varying firing rate (Wills et al., 2005; Niessing and Friedrich, 2010; Aschauer et al., 2022). Similar to such a study (Aschauer et al., 2022) we observed groups of neurons (referred to as 'response modes', Figure 1.9C-E) that jointly increased their firing rates in response to various pure tones. With shifts in stimulus frequency, these groups appear to show either step-wise (Figure 1.9E) or more gradual response shifts (Figure 1.9C). Step-wise changes of group composition have been interpreted as a sign of nonlinear properties reflecting the formation of ensembles (e.g., Aschauer et al. (2022)). However, an alternative interpretation is that the observation of distinct 'response modes' simply reflects co-activation due to the overlap between receptive fields along the tonotopic axis. The observed seemingly step-wise transition from one 'response mode' to the next with changes in stimulus frequency likely reflects best-frequency discontinuities in the tonotopic organization (see our Figure 1.1A; Imaizumi et al. (2004)). Additionally, assessing co-activation based on firing rate alone is only a very limited basis for the identification of neurons that functionally cooperate. This is especially noteworthy when using larger bin-widths, as is used in calcium imaging approaches. A more stringent criterion, that of tight temporal synchrony, as utilized here, can help differentiating between neuron groups based on coincidental co-activation ('response modes') and groups based on synchronous co-activation ('coordinated ensembles') (Figure 1.9F). This preliminary analysis revealed that neurons grouped

16

by firing rate alone do not appear to substantially coincide with neurons grouped based on temporally aligned co-activation.

1.3   Discussion

This study aimed to investigate whether the auditory thalamus (MGB) contains cNEs with enhanced information properties, similar to those observed in A1. Our results confirm the presence of cNEs in the MGB, with consistent compositions across various, but especially smaller, bin sizes and stable structures across different stimulus conditions. Importantly, coordinated spikes among cNE member neurons exhibit higher reliability and convey more stimulus-related information than individual neurons. Neuronal groups formed by shared firing-rate changes to stimuli appear not to be congruent with cNEs. Furthermore, our findings demonstrate that cNEs are not the result of false positive detection or byproducts of slow state oscillations in anesthetized animals. These findings provide support for the notion that synchronized neuronal ensembles represent a general principle of local organization for information processing in the auditory forebrain.

cNEs are ubiquitous in local circuit organization

Neuronal ensembles were proposed as fundamental units for information processing in the brain (Hebb, 1949; Buzsáki, 2010),, supported by evidence of precise temporal coordination in cortical columns (Atencio and Schreiner, 2013; See et al., 2018; Lankarany et al., 2019). Cortical columns consist of neurons with fairly homogeneous properties maintained through intracortical processing and shared afferent input (Mountcastle, 1997). This raises the question of whether cNEs are unique to cortical organization or represent a general organizational and information processing unit along sensory pathways. In the auditory system, reciprocal connectivity exists between the MGB and A1, with convergence of frequency tuning and spectral and temporal modulation preferences, preserving topographic organization in both regions (Miller et al., 2001, 2002; Bartlett and Wang, 2007; Read et al., 2011). Therefore, investigating neuronal coordination in the MGB, where neurons possess similar properties but differ in their organizational and

17

cytoarchitectonic patterns from A1 (Winer, 2010), can provide insights into whether cNEs are general organizational principles of local circuits or specialized units specific to the cortical circuit composition.

We conducted recordings of neuronal activity across multiple iso-frequency layers of the MGB and were able to reliably detect cNEs in MGB (Figure 1.2). Neurons within the same cNE displayed closer spatial proximity and shared more similar tuning properties (Figure 1.5D and E), indicating functional coherence within cNEs. It is important to note that our recordings were limited to relatively small populations of 10-30 neurons due to the techniques employed. Therefore, the confinement of spatial and frequency tuning properties within cNEs may vary when larger populations with hundreds or thousands of neurons are recorded.

We further demonstrated that the identification of cNEs relies on the temporal coordination among neurons. When the original temporal order among neurons was disrupted through circular shuffling of spike trains, a significantly lower number of cNEs were detected in both the MGB and A1 (Figure 1.4F and 1.7D). Moreover, the few false positive cNEs that were identified did not exhibit the properties observed in cNEs identified in the real data, such as stability across different stimulus conditions (Figure 1.4E and 1.7E). These findings provide strong support for the critical role of temporal coordination in the formation and characterization of cNEs in the auditory thalamus and cortex.

Time scale of cNEs

Previous studies have investigated neuronal synchrony and coordination across widely differing timescales, ranging from a few milliseconds (Lankarany et al., 2019; Shahidi et al., 2019; El-Gaby et al., 2021) to several hundred milliseconds (Miller et al., 2014; Tremblay et al., 2015; Filipchuk et al., 2022). The selection of a specific timescale in these studies was influenced by various factors, including the temporal resolution of the recording methods used, the targeted functional timescale, and the inter-neuronal distance under investigation. In the context of auditory processing, where information changes rapidly within tens of milliseconds (Rosen, 1992;

Lewicki, 2002), we specifically chose a temporal resolution of 10ms. This choice aligns with the timescale at which auditory information operates and holds relevance for synaptic integration. Selecting an appropriate timescale is crucial for future investigations into the functional role of cNEs in synaptic transmission within the auditory thalamocortical system.

We have demonstrated the robustness of cNE identification across different time bin sizes (Figure 1.3), which can be attributed to the sparse nature of neural activity. Since most synchronized neuronal firing occurs at frequencies below 10 Hz (O'Connor et al., 2010), the choice of time windows, whether 10ms or 20ms, has minimal impact on the observed correlations among neurons. However, it is important to note that cNEs identified with longer time resolutions (hundreds of milliseconds) may significantly differ from those identified with shorter resolutions (tens of milliseconds). Specifically, cNEs identified with larger time bins may falsely include 'synchronous' events from bursting or rebound activity rather than from an initial period that dominates the transmission of stimulus-triggered information. Long synchronization windows may also include neurons displaying weaker synchronization within short time windows, while potentially de-emphasizing neurons with high temporal precision in synchrony (Figure 1.3D). Hence, the chosen temporal resolution influences the composition and properties of cNEs, emphasizing the importance of selecting the appropriate timescale for studying neural ensembles.

Stability of cNEs for spontaneous and evoked activity

Our study revealed that a significant proportion of cNEs (55% in MGB and 76% in A1) maintained a consistent composition during both spontaneous and sensory-evoked neural activity (Figure 1.4E and 1.7E). This suggests that cNEs generally represent stable configurations within local circuits that can manifest independently of stimulus-driven synchrony. These findings align with previous research demonstrating similarities between patterns observed in spontaneous and stimulus-driven activity (Luczak et al., 2009). Moreover, the similarity between MGB and A1 cNEs indicates that functional network units are not limited to cortical organization but likely exist as a common modality across multiple stages of the sensory pathway.

cNEs enhance stimulus encoding

Considering that cNEs were observed in both spontaneous and stimulus-driven activity, some argue that they are merely a reflection of background activity and not involved in stimulus encoding and even potentially impairing it (Zohary et al., 1994; Abbott and Dayan, 1999; Jermakowicz et al., 2009). Contrary to this notion, our observations revealed that cNE spikes exhibit a higher signal-to-noise ratio and convey more information per spike when compared to the entire spike train (Figure 1.6B and C). This suggests that cNE events are more stimulus-selective than the contributing neurons (See et al., 2021) and exhibit a more reliable response to the stimulus features represented by the cNE STRF. The stable connectivity pattern revealed by spontaneous, intrinsic activity likely reveals aspects that have been imprinted by extensive experience and the behavioral relevance of the associated functional preferences.

Additionally, we observed an enhanced information encoding in cNE groups and cNE spikes when compared to non-cNE groups or coincident spikes, with control of the total number of neurons in the groups (Figure 1.6B and C). This observation suggests that the information increase relies on the coordination among cNE member neurons, rather than being a simple result of independent population coding (deCharms, 1998; Hatsopoulos et al., 1998).

Correlated spikes can enhance the transmission of salient auditory information by synchronously converging onto their targets (Stevens and Zador, 1998; Zandvakili and Kohn, 2015). Additionally, neurons exhibit a multiplexed nature of stimulus encoding, where spikes from the same neuron can carry information related to distinct stimulus aspects (Walker et al., 2011; Lankarany et al., 2019; See et al., 2021). The function of cNEs may involve selectively choosing spikes from member neurons that are most relevant for a specific target information and enhancing information propagation while excluding functionally irrelevant spikes of the same neurons. This mechanism significantly improves both the robustness and capacity of information encoded within a population of neurons (Walker et al., 2011; See et al., 2021). Thus, the presence of cNEs and their coordination within a neuronal population can facilitate efficient information

processing and transmission in the auditory system. Future studies involving simultaneous recordings from two stations along the auditory pathway will be necessary to test this hypothesis.

cNE formation does not depend on strong slow oscillations

Slow oscillations are commonly observed in neural activity during anesthesia (Chauvette et al., 2011; Dasilva et al., 2021) and have been shown to influence stimulus encoding (Pachitariu et al., 2015). Concerns have been raised regarding whether cNEs are solely a result of anesthesia-induced synchrony. However, our research findings refute this notion. We focused on a distinct time scale of synchronization unrelated to anesthesia-induced slow oscillations and successfully detected cNEs in recordings without strong slow oscillations. These cNEs exhibited stable structures and enhanced information properties, indicating that they are not solely a byproduct of anesthesia-induced synchrony. While we ruled out slow oscillations as the primary force underlying cNE formation, it is important to consider their potential interaction with other oscillatory activity, such as gamma rhythms (Oberto et al., 2022). Further research is needed to explore the interplay between cNEs and different types of brain oscillations.
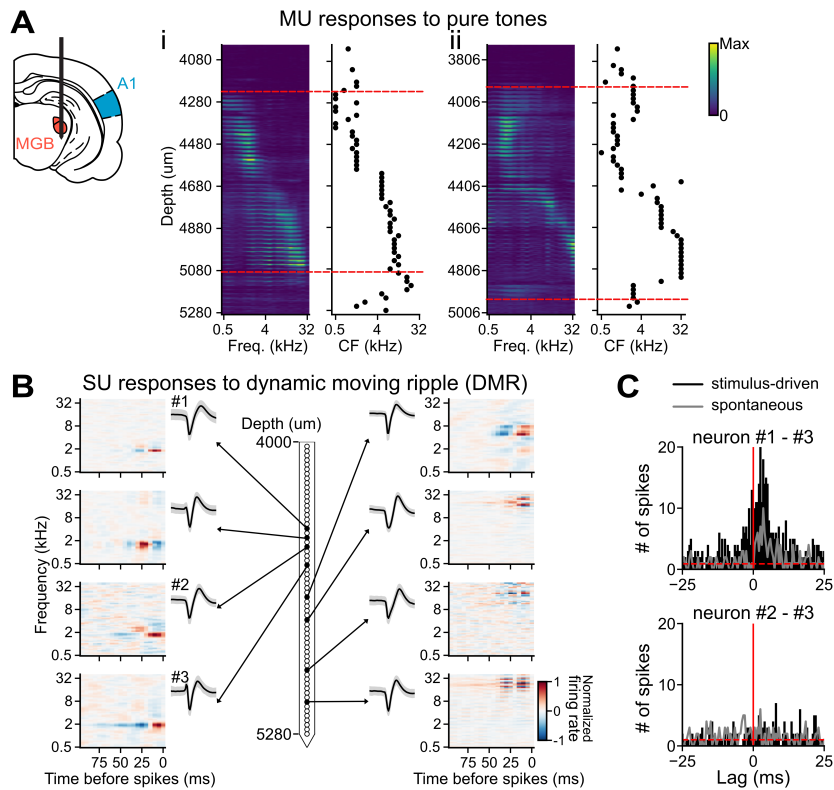
1.4 Figures

Figure 1.1

Figure 1.1: *In vivo* **recordings in rat MGB.** (A) Left: Schematic of the recording setup in the MGB using a linear 64-channel probe. (i) and (ii): two electrode penetrations with multi-unit (MU) recordings from the MGB. Left: Stacked firing rate (color coded) of pure-tone frequency response areas. Right: Characteristic frequencies (CF, the frequency at which the response threshold is the lowest). The red dashed lines indicate the potential boundaries of the ventral MGB. (B) Example STRFs of SUs from a recording in the MGB. Unit numbers 1 to 3 indicate the positions and STRFs of pairs of neurons whose CCGs are plotted in (C). (C) Example CCGs from two pairs of neurons (#1 - #3 and #2 - #3). The black bars represent the CCGs of stimulus-driven activity, while the grey lines represent the CCGs of spontaneous activity. The baseline is estimated by averaging the counts in 5ms windows at the shoulders of the CCGs and is indicated by dashed red lines.
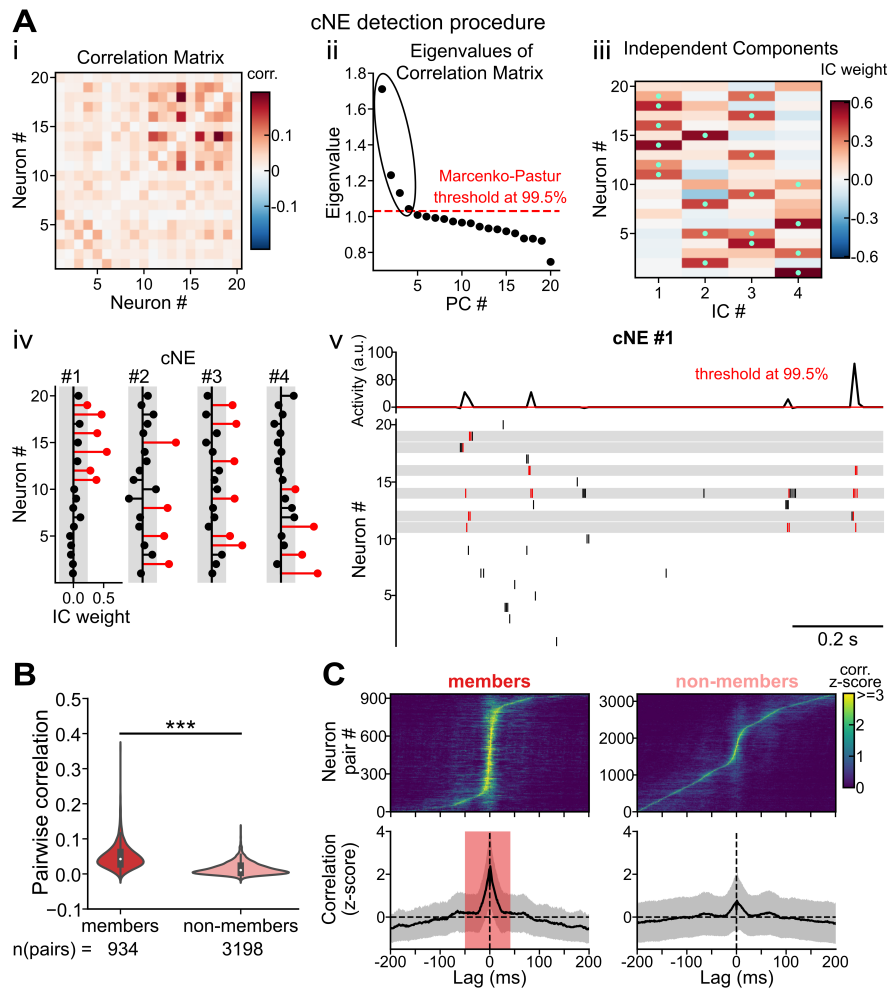
Figure 1.2

Figure 1.2: **Groups of neurons with coordinated activities exist in MGB.** (A) Procedures for detecting cNEs in a thalamic penetration. (i) Correlation matrix of spike trains. (ii) Eigenvalues of the correlation matrix shown in (i). The dashed red line represents the 99.5th percentile of the Marčenko-Pastur distribution, which was used as the significance threshold for eigenvalues. The top four eigenvalues are significant and represent the number of detected cNEs. (iii) IC weights of neurons for each cNE. The green dots represent neurons that are members of a cNE. (iv) cNE members (red stems) are neurons with IC weights exceeding the threshold ($1/\sqrt{N}$) shown as grey areas. (v) Example of cNE activation. Top: Activity trace of cNE #1. The red line shows the threshold estimated using Monte Carlo methods. The peaks crossing the threshold indicate cNE events when multiple cNE member neurons fire jointly. Bottom: Spike raster of neurons, with red ticks indicating spikes that contribute to instances of cNE events, which were referred to as cNE spikes. Shaded areas show member neurons. (B) Correlations (10ms bin) of neuron pairs that were both members of the same cNE (members) or neuron pairs that were not members of the same cNE (non-members) in MGB ($p = 6.9\text{e-}235$, Mann–Whitney U test). (C) Z-scored CCGs (1ms bin) of member pairs (left) and non-member pairs (right) in MGB. Top: Stacked CCGs ordered by the peak delay. Bottom: Average of the data above (mean $\pm$ SD; shaded area: $p < 0.01$, permutation test, shuffling the members/non-members labels).

Figure 1.3

A cNEs identified on different bin sizes that best match the cNEs identified on 10ms bins

i cNE with stable IC weights across bin sizes

ii cNE detected only on small bin sizes

B Changing of detected cNEs with bin sizes

C Correlation of IC weights and proportion of shared membership of 10ms cNEs with 160ms cNEs

D

E member neurons in both 10ms and 160ms cNEs
member neurons in the 10ms cNE
member neurons in the 160ms cNE

neurons identified as members of a cNE using 10ms bins

neurons identified as members of a cNE using 160ms bins

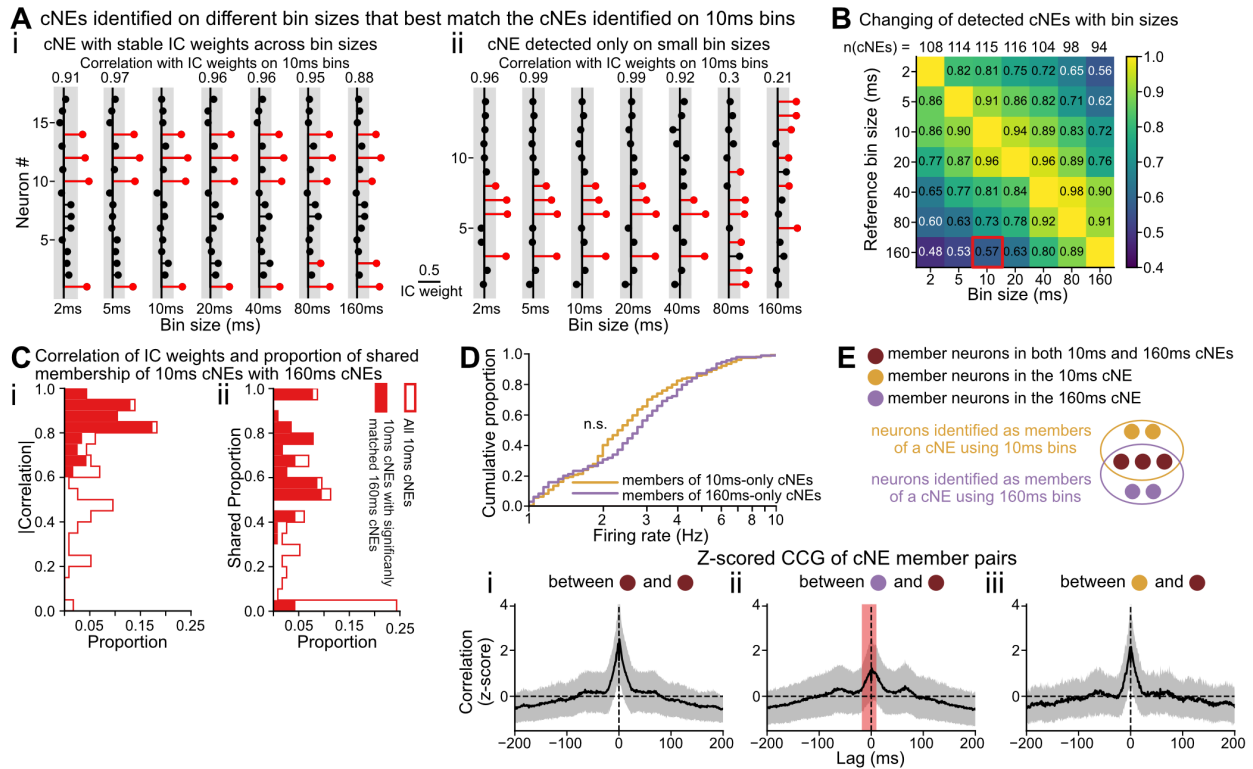Z-scored CCG of cNE member pairs

Figure 1.3: Variability of IC weights across different time bin sizes. (A) Example of two MGB cNEs whose member neurons are either consistently identified across different bin sizes (i) or only detected using smaller bin sizes (ii). (B) Proportion of significantly matched cNEs. Using different bin sizes as reference bin sizes (row), we calculated the proportion of cNEs on different bin sizes that have a significantly matched cNE on the reference bin size. The red square highlights the proportion of 10ms cNEs that have significant matches with 160ms cNEs and is further analyzed in (C). (C) Left: Correlation of IC weights of 10ms cNEs with the most correlated IC weights of 160ms cNEs. Right: Proportion of shared membership between 10ms cNEs with their most correlated 160ms cNEs. (D) Firing rate of member neurons in 10ms-only cNEs, 10ms cNEs without a significant match with 160ms cNEs, and 160ms-only cNEs (p = 0.57, Kolmogorov-Smirnov test). (E) Top: Schematic of membership of neurons for different bin sizes. Bottom: Mean z-scored CCGs (1ms bin, mean $\pm$ SD) between (i) member neurons in both 10ms and 160ms cNEs, (ii) member neurons only in the 160ms cNE and member neurons in both 10ms and 160ms cNEs (shaded area: p < 0.01, permutation test, shuffling neuron pair labels of i and ii), and (iii) member neurons only in the 10ms cNE and member neurons in both 10ms and 160ms cNEs (no time bin showed significant difference from i)
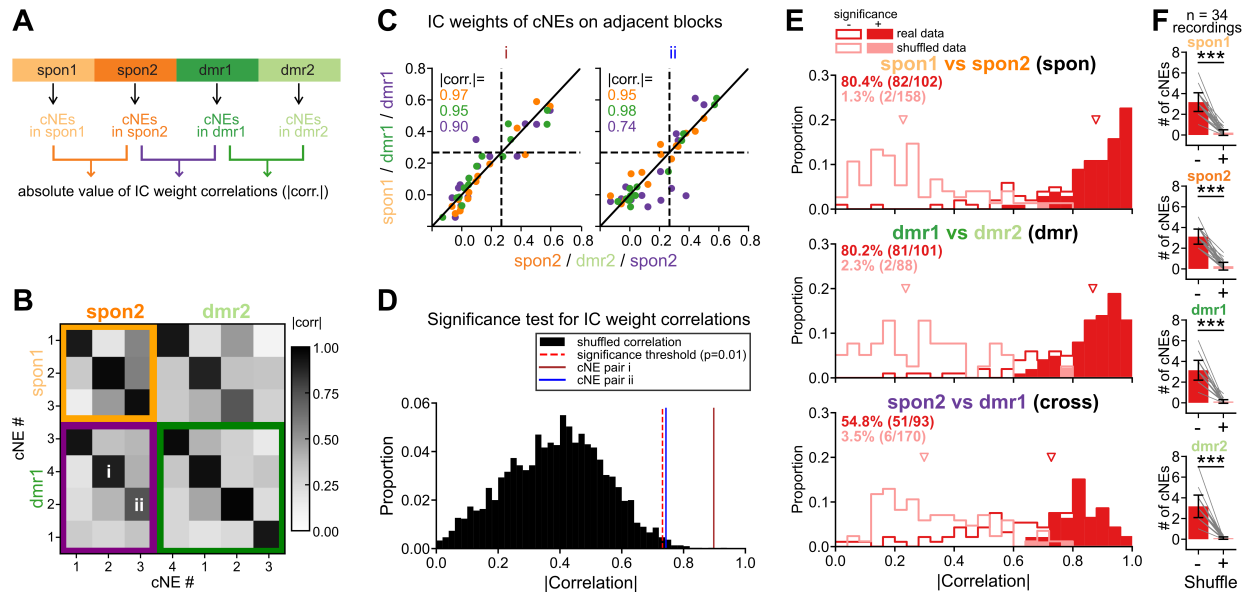
24

Figure 1.4

Figure 1.4: cNEs identified in spontaneous activity are mostly preserved in stimulus-driven activity. (A) Diagram illustrating the recording sequence and partitioning of spontaneous (yellow/orange) and DMR-evoked (dark green/light green) activity. The four blocks allowed the comparison of cNEs obtained within stimulus conditions and across stimulus conditions. (B) Absolute correlation values of the IC weights calculated on adjacent blocks from an MGB recording including the two examples (i and ii) shown in (C). (C) Example IC weights on adjacent blocks with high (i) and moderate (ii) correlation values across stimulus conditions. The dashed lines show the threshold to determine the membership of the neurons. (D) The two cNE examples in (C) have significantly matched IC weights across stimulus conditions. See method for how the null distribution was generated. The significance threshold for the correlation values was set at p = 0.01 (red dashed line, 99.5th percentile of the null distribution). The brown (i) and blue (ii) solid lines represent the two examples in (C). (E) Correlations of IC weights identified on adjacent activity blocks for real (red) and circularly shifted data (pink). The hollow histograms show all correlations of matched cNEs on adjacent blocks; the histograms show significant correlations based on the test shown in (D). The inset numbers show the percentage of cNEs with significantly matched IC weights on adjacent blocks. The triangles show the median of all IC weight correlations (real data vs shuffled data: spon, p = 5.6e-36; dmr: p = 1.3e-28; cross, p = 2.0e-22, Mann–Whitney U test with Bonferroni correction). (F) Number of cNEs detected using real and circularly shifted activities on the four recording blocks (spon1, p = 4.7e-10; spon2, p = 4.7e-10; dmr1, p = 4.7e-10; dmr2, p = 4.7e-10, Wilcoxon signed-rank test with Bonferroni correction).
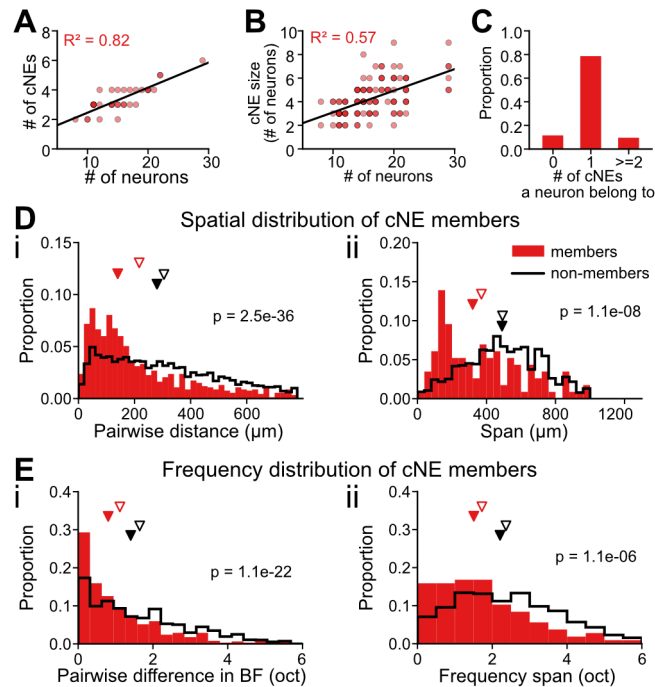
Figure 1.5

Figure 1.5: Properties of cNEs in MGB. (A) Number of cNEs detected in any given penetration increases with the number of recorded neurons. (B) cNE size increases with the number of recorded neurons. (C) The number of cNEs a neuron belongs to. (D) Spatial distribution of cNE members. (i) Pairwise distance of neurons in the same cNE (colored bar) or neurons not in the same cNE (black line). (ii) Spatial span of cNE members (colored bar) and random groups of neurons with the same number of neurons as cNEs (black line). (E) Frequency tuning distribution of cNE members. (i) Pairwise difference in the best frequencies (BF) of neurons. (ii) The largest difference in the BF among cNE members or random groups of neurons. (Mann–Whitney U test).
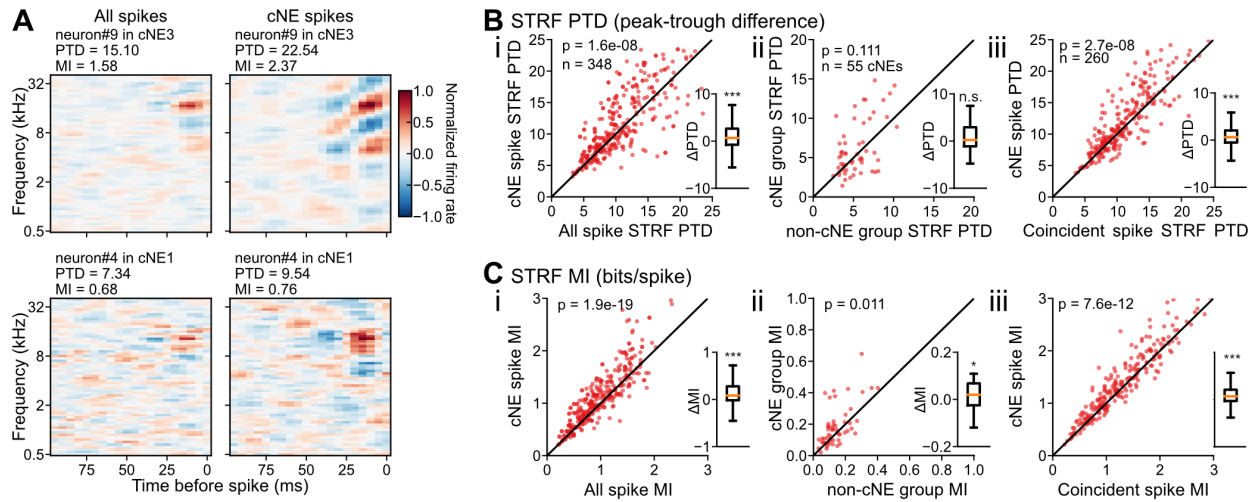
Figure 1.6

Figure 1.6: **MGB cNEs can refine sound features encoded by member neurons.** (A) Two example STRFs of MGB neurons calculated with all spikes (left) and cNE spikes (right). All spikes are subsampled to have an equal number as cNE spikes. (B) (i) STRF PTD for cNE spikes or all spikes of neurons. (ii) STRF PTD for groups of cNE members or non-members. (iii) STRF PTD for cNE spikes and coincident spikes of a neuron. The coincident spikes refer to instances where a neuron's firing occurs within a 10ms time frame of another neuron's firing in a group of non-member neurons. This group is designed to match the number of neurons present in the cNE. (C) (i) MI between stimulus and cNE spikes or all spikes of neurons. (ii) STRF MI for groups of cNE members or non-members. (iii) STRF MI for cNE spikes and coincident spikes of a neuron. (Wilcoxon signed-rank test).
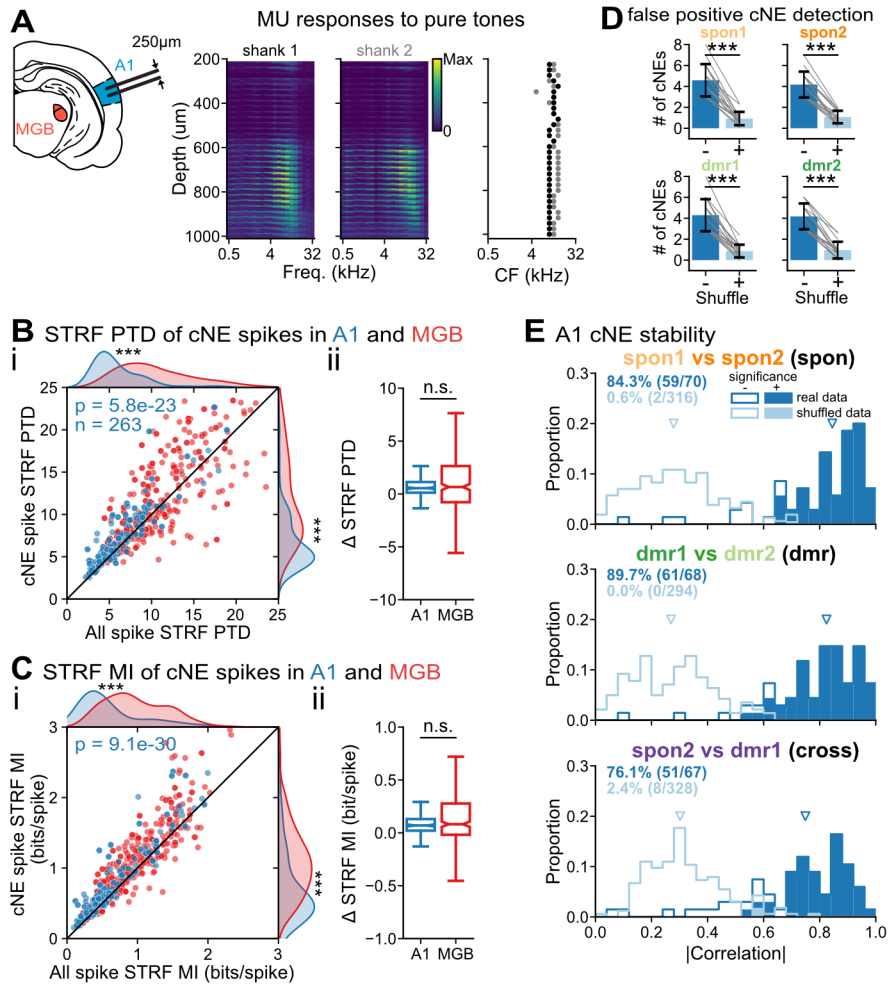
Figure 1.7

Figure 1.7: MGB and A1 cNEs have similar properties. (A) Left: schematic of the recording setup in A1 using a 2-shank probe with 64 channels. Right: MU responses to pure tones as in Figure 1.1A. (B) (i) PTD of STRFs calculated using all spikes or only cNE spikes from a neuron in A1. (ii) Difference between cNE spike STRF PTD and all spike STRF PTD in MGB and A1 (p = 0.72, Mann–Whitney U test). (C) (i) MI of STRFs calculated using all spikes or only cNE spikes from a neuron in A1. (ii) Difference between cNE spike STRF MI and all spike STRF MI in MGB and A1 (p = 0.92, Mann–Whitney U test). (D) Number of cNEs detected using real and circularly shifted activities on the four recording blocks in A1, as shown in Figure 1.4F for MGB. (spon1: p = 6.1e-5, spon2: p = 6.1e-5, dmr1: p = 6.1e-5, dmr2: p = 6.1e-5, n = 17 recordings, Wilcoxon signed-rank test with Bonferroni correction). (E) Correlations of IC weights identified on adjacent activity blocks for real (blue) and circularly shifted data (light blue) in A1. The hollow histograms and histograms show the distribution of correlations and significant correlations as in Figure 1.4E. The triangles show the median of IC weight correlations (spon: p = 1.4e-33, dmr: p = 4.6e-34, cross: p = 4.8e-28, Mann–Whitney U test with Bonferroni correction).
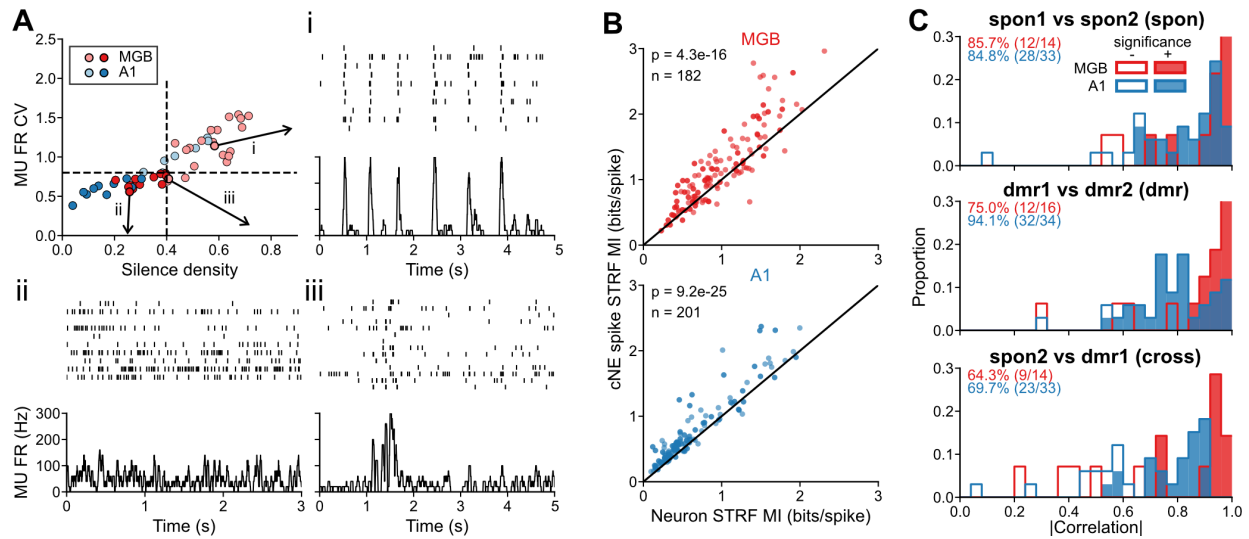
Figure 1.8

Figure 1.8 cNE events do not rely on slow oscillation in neural activity. (A) Silence density and firing rate (FR) CV of population activity in response to DMR. Some recordings show strong slow oscillation in population activity with pronounced silent period between highly active moments (i), while others show little (ii) or moderate (iii) levels of slow MU firing rate oscillation. Recordings with silence density <0.4 and MU firing rate coefficient of variance <0.8 (dashed lines) did not show prominent slow oscillation in population activity and were included in (B). (B) STRF MI with all spikes and cNE spikes in recordings without prominent slow oscillations (Wilcoxon signed-rank test). (C) Correlation values of cNE IC weights on adjacent activity blocks from recordings with no prominent slow oscillations in both spontaneous and stimulus-driven activities. The inset numbers show the percentage of cNEs with significantly matched IC weights on adjacent blocks in MGB (red) and A1 (blue). The hollow histograms and histograms show all correlation values and significant correlation values with the same presentation scheme as in Figure 1.4E.
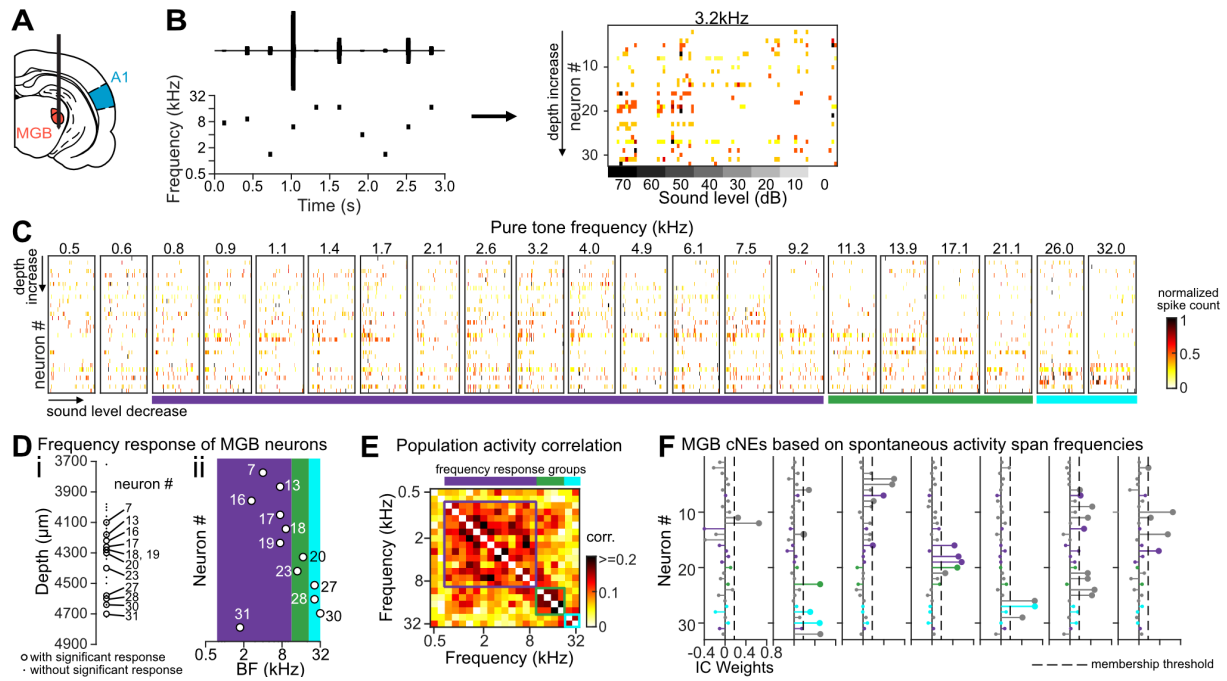
Figure 1.9

Figure 1.9 MGB cNEs are not congruent with firing-rate based neuronal groups. (A) Schematic of a recording in the MGB. (B) Left top: The waveform of pure tone stimuli that vary in frequency and intensity over a 3s interval, Left bottom: Stimulus frequency sequence in the 3s interval. The pure tones cover frequencies from 0.5 to 32 kHz in 0.29 octave steps and sound levels from 0 to 70 dB in 10 dB steps (50ms, 5ms ramps). Each frequency-sound level combination was presented 10 times in a pseudo-random order, with an inter-stimulus interval of 250ms. Right: Population response pattern to pure tones at 3.2 kHz. The response of each neuron to a pure tone was measured by the number of spikes within 50ms after stimulus onset. The response amplitude was normalized by the largest response in each neuron. Trials were ordered by sound level from left to right, and neurons were ordered by depth from top to bottom. (C) Population response patterns in an example recording to pure tones. The colored bars below correspond to the neuron groups in (D), reflecting similar frequency response preferences. (D) Location and BF of MGB neurons in the example recording. (i) Depth of neurons from the surface of the cortex. The open circles indicate MGB neurons with significant responses to pure tones; the dots indicate MGB neurons without significant responses. The significance was determined by comparing the number of spikes fired in the 50ms window before and after stimulus onset (Wilcoxon signed-rank test, p <0.01). (ii) Best frequencies of MGB neurons with significant responses to pure tones. The best frequency was calculated by summing responses to pure tones at the same frequency and different sound levels. The frequency with the largest response followed is the best frequency of the neuron. The background color corresponds to neurons that co-vary in their firing rate to the pure tones (see Panel E). (E) Correlation of population activity in response to pure tones of different frequencies. Colored squares represent the frequency range shared by a group of neurons as in (D). (F) MGB cNEs based on spontaneous activities. Multiple cNEs consist of neurons without significant responses to pure tones, indicated in gray, and neurons with different frequency preferences, indicated in different colors as in (D).

30

Chapter 2: Auditory Thalamocortical Transmission Enhanced by Ensemble Activity

2.1   Introduction

Neurons in the forebrain and other brain structures have been shown to be highly interconnected (Braitenberg and Schutz, 1991; Anderson et al., 2007). As a consequence, the activity of individual neurons can be strongly correlated with some of its neighbors, and this coordinated activity is thought to underlie information processing throughout the brain by supporting various processes, such as perception, memory formation, and decision making (Bathellier et al., 2012; Gulati et al., 2014; Kiani et al., 2014; Jacobs et al., 2015; DeNardo et al., 2019). These neuronal ensembles, defined as groups of neurons with reliable and precise synchrony, have been proposed as a fundamental unit for information processing in the brain (Harris, 2005; Buzsáki, 2010; Yuste, 2015). In the auditory thalamus and cortex, the activity of cNEs has been shown to be stable functional constructs (See et al., 2018, 2021). They are present in both spontaneous and evoked activity and encode more information about an auditory stimulus than single neurons or random groups of simultaneously recorded neurons (Averbeck et al., 2006; Montijn et al., 2016; Lankarany et al., 2019; See et al., 2021).

For ensemble encoding of stimuli to serve as a neural code, however, it is necessary that the encoded signal be effectively transmitted to downstream brain areas, enabled by connectional convergence of the ensemble members on a target neuron. Previous studies have illuminated some aspects of the relationship between sensory thalamic neurons and their target cells in cortex. Examining the extent to which auditory cortical receptive fields are directly inherited from their thalamic inputs showed that some cortical receptive field properties are faithfully propagated whereas others are significantly transformed (Miller et al., 2001). Furthermore, thalamic spikes that drive the auditory cortex are generally more selective for spectrotemporal stimulus features than spikes from the same neuron that do not drive the cortex (Miller et al., 2001). This suggests

that not every spike of a thalamic spike train in response to a time-variant stimulus encodes the same information, or, alternatively, is ineffective and requires convergent, coinciding input to drive the cortical activity. Thalamocortical synapses have generally low efficacy (Bruno and Sakmann, 2006). It has been shown, however, that closely timed homosynaptic and heterosynaptic thalamic inputs can be summed to strongly excite cortical cells (Alonso et al., 1996; Roy and Alloway, 2001; Swadlow and Gusev, 2001; Bruno and Sakmann, 2006). This suggests that synchronized, heterosynaptic ensemble input can provide a stronger drive to excite a target neuron and, thus, provides more robust information transmission. However, due to the difficulty in conducting simultaneous recordings across multiple brain areas, there is limited experimental support for the effects of ensemble activity on the transmission of signals to downstream neurons.

To investigate this, we identified pairs of functionally connected neurons in the MGB and A1 based on their spontaneous activities. Notably, spikes from MGB neurons in synchrony with other members in the same cNE ("cNE spikes") exhibited higher efficacy in driving A1 neuron firing, compared to spikes unrelated to cNE activities ("non-cNE spikes"). The increased efficacy of cNE spikes were only observed when the A1 target neuron was narrow-spiking but not when the A1 target neuron was broad-spiking. In addition, the increased efficacy of cNE spikes were specific to particular A1 target neurons, rather than resulting in a general increase in the firing rate across all tested A1 neurons. These findings support the notion of neuronal ensembles with coordinated activity as functional units that enhances information encoding as well as transmission in the brain.

2.2   Results

Efficacy of Functional Connectivity from MGB to A1.

We performed 125 pairs of simultaneous recordings in the rat MGB and A1 (Figure 2.1A). STRFs were assessed using DMR, a broadband noise with varying spectral and temporal modulation rates over time. To identify a potential functional connection, we cross-correlated the spike trains from all simultaneously recorded MGB and A1 neurons. Functionally connected thalamocortical

neuronal pairs are characterized by a sharp peak with short latency (1-5ms) in their cross-correlograms (CCGs) (Figure 2.1B-i) (Tanaka, 1983; Clay Reid and Alonso, 1995; Miller et al., 2001). Typically, functionally connected MGB and A1 neuron pairs demonstrate some degree of overlap in the frequency preference and a short delay of cortical versus thalamic responses (Figure 2.1B-ii) (Miller et al., 2001). We identified 68 pairs of MGB and A1 neurons as functionally connected based on their spontaneous activity, comprising 46 unique MGB neurons and 31 unique A1 neurons, from 12 recordings in 7 animals.

To quantify the efficacy of spikes from an MGB neuron in driving an A1 neuron firing, we used the ratio of "causal spikes", i.e., those thalamic spikes that were closely followed by a cortical spike, to the total number of thalamic spikes. The CCG expresses the number of A1 spikes in their temporal relationship to thalamic spikes. From the CCG, we can identify the subset of A1 spikes potentially resulting from thalamic spikes, i.e., the causal MGB spikes. The count of causal spikes was determined within the 4ms range around the CCG peak, excluding the baseline estimated from the 4ms range immediately before and after the peak. On average, approximately 5% (median: 4.67%, mean: 5.97%, SD: 5.25%) of spikes from a given MGB neuron led to a spike in a connected A1 neuron during spontaneous activity (Figure 2.1C). Among the 68 neuronal pairs, 15 pairs also exhibited a significant peak in their CCG during stimulus driven activity. There was no significant difference in efficacy resulting from spontaneous and stimulus driven CCGs (p = 0.80, Mann–Whitney U test. median: 3.97%, mean: 6.04%, SD: 5.91%). However, in pairs with significant CCGs under both conditions, the spontaneous efficacy (median: 6.14%, mean: 9.22%, SD: 8.60%) was significantly higher than the stimulus-driven efficacy (p = 0.012, Wilcoxon signed-rank test). This difference may stem from a bias toward neurons with higher spontaneous firing rates, as the significance of the CCG peak requires a substantial number of events. Indeed, both MGB and A1 neurons in the identified functional connections exhibited higher spontaneous firing rates than stimulus-driven firing rates (MGB: p = 0.002, A1: p = 0.022, Wilcoxon signed-rank test) (Figure 2.1D).

To verify that functionally connected thalamocortical neuronal pairs show similar response preferences as reported in previous studies (Clay Reid and Alonso, 1995; Miller et al., 2001), we compared the best frequencies of neurons with significant STRFs (Figure 2.1E). Among the 15 pairs of MGB and A1 neurons exhibiting significant CCGs in both spontaneous and stimulus-driven activity, 11 pairs showed significant STRFs in both MGB and A1 neurons in response to DMR. These pairs demonstrated an average absolute difference of 0.33 ($\pm$0.28) octaves between the best frequencies of the MGB and A1 neurons. Among the remaining 53 pairs, 38 exhibited significant STRFs in both the MGB and A1 neurons despite lacking a significant stimulus-driven CCG. These pairs of neurons displayed a comparable difference in their best frequencies (0.53 $\pm$ 0.69 octaves, p = 0.83, Mann-Whitney U test). In general, functionally connected MGB and A1 neurons had similar but rarely identical frequency preferences confirming previous observations (Miller et al., 2001).

MGB neurons with synchronous activities are more likely to connect to the same A1 neuron.
The functionally connected neuronal pairs, along with other neurons within the same recordings, presented an opportunity to investigate the relationship between activity correlation in the MGB and their connectivity to A1 neurons. To mitigate confounding factors arising from stimulus-driven synchrony, our analysis focused solely on spontaneous activities. It has long been proposed that cortical neurons primarily operate as coincidence detectors, sensitive to the simultaneous arrival of spikes from multiple inputs within a brief temporal window (König et al., 1996; Salinas and Sejnowski, 2001; Roy and Alloway, 2001; Bruno and Sakmann, 2006; Kumar et al., 2010). This implies a necessity for high correlated firing among input neurons to drive a common target firing. Consider three example neurons in our recordings (Figure 2.2A-i), where neuron #1 and neuron #2 share a common A1 target, while neuron #1 and neuron #3, despite similar frequency tuning (Figure 2.2A-ii), do not. We observed synchronized firing between #1 and neuron #2, in contrast to only a small correlation between neuron #1 and neuron #3 (Figure 2.2A-i). Further analysis of pairwise correlation among MGB neurons at a 10ms resolution, chosen to align with the synaptic integration window of most cortical neurons (Léger et al., 2005;

D'amour and Froemke, 2015), revealed a significantly higher correlation among MGB neurons sharing a common A1 target compared to those without a common A1 target (Figure 2.2A-iii). To reduce the chance of falsely categorizing a neuronal pair as not sharing an A1 target due to limited extracellular recording sampling, only MGB neurons with identified A1 neuron targets were included in this analysis. Moreover, only recordings with at least one pair of neurons sharing an A1 target were considered (9 out of 12). The observation of high correlation among neurons connected to the same target supports the notion that correlation among input neurons plays a crucial role in enhancing transmission robustness and directing information flow to downstream neurons.

To identify groups of neurons with correlated firing in the MGB, we employed a dimensionality reduction technique (Lopes-dos Santos et al., 2011; See et al., 2018), resulting in the detection of cNEs (See et al., 2018). Consider again three neurons in an MGB recording (Figure 2.2B-i and ii): two neurons within the same cNE ("within cNE"), neuron #1 and #2, display synchronized firing, whereas two neurons belonging to the same cNE ("outside cNE"), #2 and #3, exhibit little correlation in their activity. To validate that cNEs accurately capture groups of neurons with correlated firing in the MGB, we compared the pairwise correlation of MGB neurons based on whether they were within or outside cNEs (Figure 2.2B-iii). The analysis revealed a significantly higher correlation among MGB neurons within the same cNE compared to those located outside cNEs. This result affirms that cNEs effectively describe groups of neurons with synchronous activities in the MGB.

Given that MGB neurons sharing an A1 target exhibit higher correlation and that cNEs delineate groups of MGB neurons with correlated firing, the question arises whether two neurons identified as members in the same cNE, displaying correlated firing, are more likely to connect to the same A1 neuron compared to MGB neurons not in the same cNE (Figure 2.2C). To address this, we compared the probability of pairs of randomly drawn MGB neurons connecting to the same A1 neuron, conditioned on whether the two neurons are members of the same cNE or not (Figure

35

2.2C-i). The result shows that MGB neurons in the same cNE are indeed more likely to connect to the same A1 neuron (Figure 2.2C-ii). The observation that cNE members tend to converge onto the same A1 target lends support to the structural foundation for cNEs to function as information transmission units.

cNE spikes are more efficacious than non-cNE spikes at driving A1 neuron firing.

Prior research has identified cNEs as a potential information encoding substrate (See et al., 2018, 2021), yet the extent to which the cNE-encoded information effectively reaches downstream neurons remains uncertain. If neurons are responsive to cNE activities, they can extract information carried by cNE events, which have been shown to be more informative than the spikes from individual neurons. Expanding on the understanding that cNE events are more informative, we investigated whether spikes related to cNE events are more likely to induce firing in downstream neurons. Take the example of an MGB cNE (Figure 2.3A-i), where two member neurons are connected to the same A1 neuron, and the A1 neuron receives input from both MGB cNE members located in layer 4/5 of the primary auditory cortex (Figure 2.3A-ii). We constructed CCGs between the cNE spikes of the cNE member neurons and the A1 neuron spike train and compared them to the CCGs of non-cNE spikes of the same neurons (Figure 2.3A-iii). We observed that both cNE members connected to the A1 neuron exhibited higher efficacy with their cNE spikes than with non-cNE spikes. This pattern holds true at a population level as well (Figure 2.3B-i), providing support for the role of cNEs in facilitating information transmission.

To further validate the finding that cNE spikes, compared to non-cNE spikes of the same neurons, are more effective at driving A1 neuron firing, we conducted rigorous control analyses. First, we down-sampled the cNE spikes and non-cNE spikes to the same number, and the result remained consistent (Figure 3.3B-ii). This ensures that the observed higher efficacy of cNE spikes is not simply a consequence of the different numbers of spikes involved in generating the two CCGs. Second, to mitigate the impact of intracellular spike interactions, e.g., due to bursting (Usrey et al., 2000; Swadlow and Gusev, 2001), we excluded double-spikes (inter-spike interval <20ms)

from our analysis (Figure 2.3B-iii). Even after considering only single spikes fired by MGB neurons, cNE spikes exhibited higher efficacy than non-cNE spikes. Lastly, to address the concern that the heightened efficacy of cNE spikes might reflect a population effect of synchronized activities in the MGB, we compared the efficacy of cNE spikes and spikes from the same neuron that are coincident with neurons outside the cNE (Figure 2.3B-iv). The results consistently demonstrated that cNE spikes have significantly higher efficacy compared to coincident but non-cNE spikes. These findings underscore the effectiveness of cNEs as information transmission units, emphasizing their potential role in orchestrating synchronized activities in the MGB for enhanced downstream neural processing.

The transmission efficacy of MGB cNE spikes is dependent on the target cell types.

There exists a diversity of cell types in the neocortex (Noback, 1985; Markram et al., 2004). Using trough-to-peak duration (TPD) of the spike waveform as a measure, A1 neurons can be categorized as NS, putative GABAergic inhibitory interneurons, or BS, putative glutamatergic excitatory pyramidal neurons (McCormick et al., 1985; Connors and Gutnick, 1990; Nowak et al., 2003; Barthó et al., 2004) (Figure 2.4A). Given that pyramidal neurons and interneurons exhibit markedly different electrophysiological properties (Geiger et al., 1995; Hu et al., 2014), local circuit organizations (Dantzker and Callaway, 2000; Markram et al., 2004; Feldmeyer et al., 2018), and functions (Johnston et al., 2009; Atencio et al., 2008; Tsunada et al., 2012), we sought to determine if the enhanced efficacy of cNE spikes over non-cNE spikes depends on the cell type of the A1 target neuron.

Our results reveal that when an A1 neuron is NS, cNE spikes exhibit significantly higher efficacy than non-cNE spikes (Figure 2.4B). In addition, cNE spikes show higher efficacy than coincident but non-cNE spikes for NS A1 target neuron, as shown in Figure 2.3B-iv (p = 0.003, Wilcoxon signed-rank test). This effect, however, is not observed when the target is a BS A1 neuron.

Given that NS neurons tend to fire in bursts, it follows that MGB cNE spikes might trigger more bursts in A1 neurons. This occurrence is less probable in BS neurons, explaining why MGB

cNE spikes only exhibit higher efficacy towards NS A1 neurons but not BS neurons. To explore this possibility, we further investigated whether the increased efficacy of cNE spikes for NS A1 neurons results from a higher probability of MGB cNE spike in triggering A1 neuron firing, or a higher number of A1 spikes triggered by each MGB cNE spike compared to non-cNE spikes (Figure 2.4). Comparing the proportion of MGB cNE and non-cNE spikes followed by A1 neuron firing within the 1-5ms causal response window, the results showed that significantly more cNE spikes are followed by A1 neuron firing compared to non-cNE spikes in NS neurons but not when the A1 target is BS (Figure 2.4C-i). Furthermore, both cNE spikes and non-cNE spikes exhibit higher efficacy when the target neuron is NS compared to when it is BS.

We next compared the number of A1 spikes following an MGB spike when there is at least one A1 spike (Figure 2.4C-ii) to test if MGB cNE spikes, compared to non-cNE spikes, are followed by more than one A1 spike. We found, however, no significant effect of cNE and non-cNE spikes on the number of A1 spikes following an MGB spike, although more A1 spikes follow each MGB spike when the target neuron is NS compared to BS. These results show that MGB cNE spikes are more likely to trigger firing in A1 neurons, although each cNE spike does not result in more A1 spikes compared to non-cNE spikes. Thus, the tendency of NS neurons to burst does not provide an adequate explanation for the different effect of MGB cNE spikes on different types of A1 neurons.

As NS neurons typically have a higher firing rate than BS neurons (Connors and Gutnick, 1990), we explored whether the observed higher efficacy of cNE spikes for NS targets is simply a result of differences in the firing rates of the two neuron types. Regression analysis revealed no clear relationship between the difference in cNE and non-cNE spikes and the firing rate of the target neuron (Figure 2.4D). Another possibility considered was that NS neurons might integrate inputs from more MGB neurons than BS neurons, thereby requiring synchrony among MGB neurons to effectively drive activities in NS A1 neurons. To explore this, we measured the strength of MGB and A1 neuron connectivity by the contribution, calculated as the ratio of the number of causal MGB spikes to the total number of spikes in the A1 neuron. We found, however, no significant

difference in the individual MGB neuron's contribution to A1 neurons based on whether the A1 neuron is BS or NS (Figure 2.4E).

Studies have shown that preceding activities in the cortex affect the ability of thalamic inputs to drive cortical responses (Briggs and Usrey, 2007). To test whether cortical activities preceding spikes from the MGB can account for the cell-type-specific effects of MGB cNE spikes on A1 neuron firing, we compared the number of A1 spikes around MGB spikes based on A1 cell type (Figure 2.4F-i). Our analysis revealed that NS A1 neurons indeed demonstrated elevated activity both before (-150 to -50 ms, peak at -70ms) and after (50 to 90 ms, peak at 60ms) MGB spikes, exceeding two standard deviations of the baseline level. In contrast, BS A1 neurons did not exhibit similar deviations from the baseline activity level before or after MGB spikes. Comparing NS and BS neurons, we observed that the normalized activity level in NS neurons exceeded that in BS neurons 130 to 50 ms before MGB spikes. This distinction is further validated by the observation that the firing rates of NS A1 neurons within 200ms before MGB spikes were significantly higher than their average firing rate, whereas there was no significant difference in the firing rate of BS A1 neurons before MGB spikes compared to the average firing rate during the entire spontaneous activity. Additionally, we observed that while NS A1 neurons exhibited elevated activity around both cNE (-140 to -40 ms, peak at -70ms; 50 to 140 ms, peak at 70ms) and non-cNE (-150 to -50 ms, peak at -70ms; 50 to 90 ms, peak at 60ms) MGB spikes, the A1 activity level was elevated around cNE spikes than non-cNE spikes, 120 to 50 ms before and 60 to 80 ms after MGB spikes. Furthermore, both A1 and MGB neurons showed higher firing rate before cNE spikes compared to non-cNE spikes. These findings indicate that elevated network activity in the thalamocortical circuit prior MGB cNE events may contribute to increased excitability of NS A1 neurons, rendering them more susceptible to MGB inputs than BS neurons.

In summary, these results emphasized for the main thalamocortical pathway the intricate interplay between neuronal coordination of source neurons and its impact on distinct cell types of target neurons. Furthermore, they provide additional evidence that the higher efficacy of cNE spikes is

not merely a consequence of a generalized population effect.

The Divergence of MGB cNE information towards distinct A1 targets.

It has been established that an individual neuron can represent different aspects of a stimulus stream through multiplexing of information content and/or information codes (McCLURKIN and Optican, 1996; Chase and Young, 2008; Zuo et al., 2015; Madar et al., 2019; Cariani and Baker, 2022). One hypothesis regarding the enhanced information content of cNEs is that they respond only to selected portions of a multiplexed information content of its member neurons in response to an ongoing stimulus stream (See et al., 2021). This can be accomplished by tagging a relevant information portion from spike trains via coincidence with other cNE neurons and, consequently, directing them toward distinct downstream targets (See et al., 2021). If this hypothesis holds true, we anticipate that cNE spikes from a given MGB neuron would be more effective at driving firing in one particular A1 target neuron but not in another A1 neuron that is also targeted by this neuron but not by other members of this cNE. Additionally, an MGB neuron can be associated with more than one cNE, i.e., its spikes can be synchronized with one or the other cNE but not simultaneously with both. As a consequence, this neuron should carry diverse information to the different A1 target neurons of its two cNEs. With our experimental methodology, it was not feasible to obtain a sufficient sample of cNE members in the MGB that target more than one cortical neuron. Consequently, a statistically appropriate test of this hypothesis was not possible. A few individual examples, however, shall illustrate support for these hypotheses (Figure 2.5 and 2.6).

In one recording, we observed activities from an MGB cNE where multiple cNE members were connected to the same A1 neuron. Notably, one of these cNE members also targeted a second A1 neuron (Figure 2.5A-D). The A1 target neuron receiving input from multiple cNE members is likely the most efficacious receiver of the MGB cNE information, and we term this A1 neuron the "cNE-target" (Figure 2.5E). We hypothesized that cNE spikes should exhibit higher efficacy than non-cNE spikes at driving firing in the "cNE-target". Indeed, in the example MGB cNE,

where both neuron #11 and #14 are connected to the "cNE-targeted", their cNE spikes showed higher efficacy than non-cNE spikes. Additionally, however, neuron #11 was also connected to another A1 neuron, while no other cNE members displayed functional connectivity to this A1 neuron (Figure 2.5F). We consider this A1 neuron to be a "non-cNE-target". If the increased efficacy of cNE spikes were simply an effect of enhanced population activities, we would expect all A1 neurons to respond more actively to cNE spikes than non-cNE spikes. However, if cNEs function as low noise information encoding and transmission channels, we would expect that the "non-cNE-targeted" A1 neuron should not receive the information conveyed by the cNE, and thus, cNE spikes should not exhibit higher efficacy at driving firing in that A1 neuron. The result aligns with the notion that cNEs function as information encoding and transmission channels, as cNE spikes from neuron #11 did not show higher efficacy at driving firing in the "non-cNE-target" A1 neuron.

In another recording, we captured activities of an MGB neuron that was a member of two distinct MGB cNEs. Additionally, we identified an A1 neuron that was functionally connected to that MGB neuron (Figure 2.6A). For one of the two cNEs, multiple members were connected to the target A1 neuron, thus, serving to convey the information carried by that cNE. This cNE is referred to as the "A1-targeting" cNE (Figure 2.6B). cNE spikes from the "A1-targeting" cNE exhibited higher efficacy than non-cNE spikes at driving the activity of the A1 target. On the other hand, one member of the "A1-targeting" cNE also participated in a second cNE in the MGB, whose other members, however, did not converge on this A1 target neuron. This cNE is referred to as the "non-A1-targeting" cNE (Figure 2.6C). The cNE spikes of the "non-A1-targeting" cNE did not show higher efficacy at driving the A1 neuron firing. Thus, although originating from the same neuron, only spikes associated with the "A1-targeting" cNE, but not spikes that were related to the "non-A1-targeting" cNE, exhibit higher efficacy at driving the A1 target neuron. Combined, this exemplified that a given MGB neuron can robustly deliver distinct aspects of its multiplexed information content to different target neurons.

Overall, these results provide further evidence supporting the hypothesis that cNEs serve as information encoding and transmission units. Synchronization between spikes of cNE member neurons enhances the signal-to-noise ratio and, additionally, provides a more robust transmission to specific downstream targets. This is especially the case for narrow-spiking cortical targets. The observed higher efficacy of cNE spikes compared to non-cNE spikes in driving firing in "cNE-target" A1 neurons, coupled with the absence of such increased efficacy in "non-cNE-target" A1 neurons, suggests a role for cNEs in selective information transmission. These findings underscore the potential significance of cNEs, as opposed to individual neurons, as conduits for enhanced encoding and more reliable transmission of information within neural circuits.

2.3 Discussion

This study aimed to investigate whether cNEs in the MGB can transmit spikes to A1 more efficaciously than individual neurons. Our results confirm that cNE spikes from MGB neurons demonstrate higher efficacy in driving A1 neuron firing in a target-specific manner. This enhanced efficacy of cNE spikes, compared to non-cNE spikes in MGB, cannot be attributed to intra-neuronal spike interactions or coincident activities from random groups of neurons. Furthermore, our findings highlight that the enhanced efficacy of cNE spikes was observed specifically when the target A1 neuron is NS. These findings provide additional experimental support for an ensemble neural code paradigm for information curation and transmission in the central sensory system.

MGB cNEs enhanced propagation of information from MGB to A1 in a target specific way.

Ensemble activities are prevalent in various brain regions, playing pivotal roles in stimulus encoding, learning, memory, and animal behavior (Laubach et al., 2000; Baeg et al., 2003; Bizley et al., 2010; Bathellier et al., 2012; Oberto et al., 2022; Boucly et al., 2022; Domanski et al., 2023). While these studies offer compelling evidence for neuronal ensembles as fundamental units of brain activity, the effectiveness of information transmission from these ensembles to

42

downstream neurons remains elusive. Despite evidence indicating increased activities in the receiving region in response to ensemble activities in the input region (Boucly et al., 2022), the absence of identified functionally connected neurons poses a challenge in discerning whether elevated activity reflects global population changes or exhibits target specificity in ensemble activity reception.

Here we demonstrate that cNE spikes from MGB neurons, in comparison to non-cNE spikes, exhibit greater efficacy in driving activities in functionally connected A1 target neurons (Figure 2.3). The enhanced efficacy of cNE spikes cannot be ascribed to coincident spikes from random neuron groups (Figure 2.3B-iv). Moreover, there is specificity in the relationship between MGB cNEs and A1 neurons, with cNE spikes from a particular MGB cNE proving more efficacious when targeting specific A1 neurons (Figure 2.6). Similarly, an A1 neuron demonstrates greater responsiveness to cNE spikes from specific MGB cNEs, but not all MGB cNEs (Figure 2.7). These findings underscore the targeted efficacy of cNE spikes in driving downstream neuronal activities, providing experimental support for an ensemble neural code paradigm for information transmission in the central sensory system.

Cell type specific response to cNE activities.

An intriguing finding emerged as we observed that not all A1 neurons responded similarly to MGB cNE spikes. While cNE spikes from the MGB proved more efficacious than non-cNE spikes when the target A1 neuron was narrow-spiking, this enhanced efficacy was not observed in broad-spiking target A1 neurons (Figure 2.7A).

Inspired by prior studies highlighting the impact of post-synaptic activity patterns on thalamocortical communication (Briggs and Usrey, 2007), we investigated the activity of both BS and NS A1 neurons around MGB inputs (Figure 2.4F). We noted that NS neurons, in contrast to BS neurons, exhibited an elevated activity level 150 to 50 ms prior to MGB spikes. Furthermore, both NS A1 neurons and MGB neurons displayed higher activity levels before cNE spikes compared to non-cNE spikes. This heightened MGB and A1 NS activity preceding cNE events

43

suggests a potential role of thalamocortical circuit activities in the formation of MGB cNEs and the responsiveness of A1 NS neurons to cNE inputs.

Previous studies showed that cNE activities can be phase-locked to delta (4Hz) and theta (8Hz) oscillations (Oberto et al., 2022). Notably, interneurons consistently exhibited phase-locking to these oscillations, while principal neurons did not. We speculate that that brain oscillations play a pivotal role in the sensitivity of NS A1 neurons to MGB cNE spikes. However, the precise mechanism through which brain oscillations impact thalamocortical communication—whether through pre- or post-synaptic mechanisms, or a combination of both—remains undetermined. It is plausible that brain oscillations induce changes in the response threshold of A1 neurons, such as alterations in UP/DOWN states (Hay et al., 2021). Alternatively, the phase-locking of MGB cNE activities to brain oscillations may enhance A1 neuron firing, as A1 neurons integrate synchronized spikes from MGB cNE.

While categorizing A1 neurons based on spike waveforms provided insights into the effect of cNEs on different cell types, it's worth noting that principal neurons and interneurons may have overlapping waveform properties (Sukman and Stark, 2022). Future experiments employing opto-tagging could offer clarity on how different cell types might respond to ensemble activities in distinct ways.

Ensemble model for information convergence and divergence

The auditory thalamus and cortex are functionally highly interconnected (Miller et al., 2002; Bartlett and Wang, 2007). One thalamic neuron can extend its axon to cover a large area of the sensory cortex (de Venecia and McMullen, 1994). In addition, one cortical locus can receive input from multiple thalamic regions (Brandner and Redies, 1990; Huang and Winer, 2000). The complexity of this network prompts inquiries into the mechanisms governing information conversion and transmission. Previous research has demonstrated that cortical receptive fields can undergo direct inheritance from the thalamus, be constructed from smaller inputs, and be assembled through the cooperative activity of neuronal ensembles (Miller et al., 2001). Here, we

propose an ensemble model to describe the functional convergence and divergence of sensory information in the auditory thalamocortical system (Figure 2.7B). Unlike conventional approaches that focus on individual neurons, our model considers neuronal ensembles as the primary carriers of sensory information. Within this framework, each neuron functions as a multiplexed entity, capable of encoding multiple sensory features (See et al., 2021). Neurons that share encoding patterns collectively form an ensemble, firing synchronously when a common feature is detected in the stimulus. The information pertaining to such a sound feature is then propagated to cortical neurons connected to multiple members of the cNE. Importantly, a single neuron can participate in multiple ensembles, thereby is able to channel different aspects of its multiplexed sound information to diverse downstream targets. Consequently, while a single thalamic neuron may be connected to multiple cortical neurons, the response of each cortical neuron is subject to variation due to the influence of other ensemble members. Our ensemble model offers a comprehensive understanding of the intricate processes involved in the processing and transmission of sensory information within the auditory thalamocortical system.
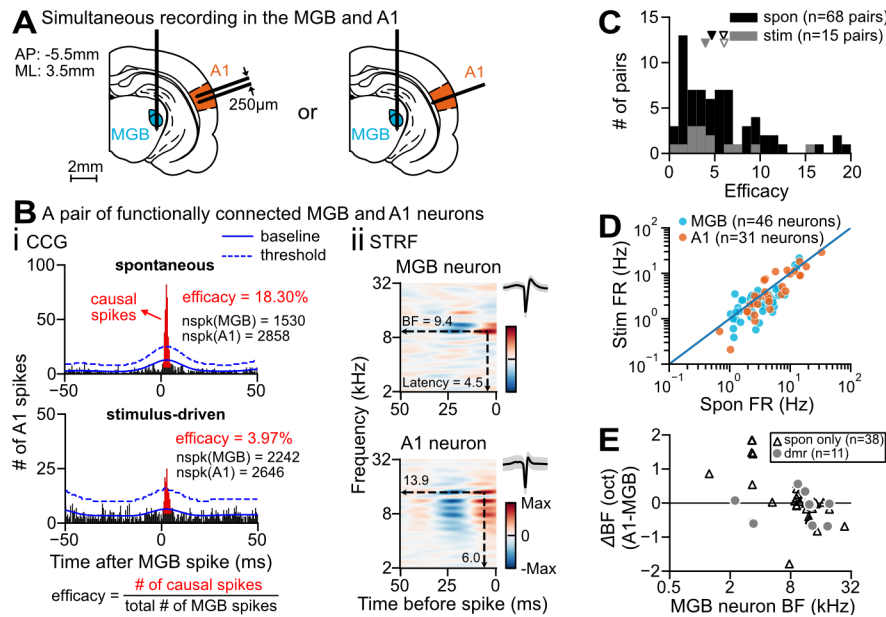
2.4 Figures

Figure 2.1

Figure 2.1 Identifying functional connectivity from MGB to A1. (A) Schematics of the recording setup in the MGB and A1. MGB: linear 64-channel probe; A1: either a two-shank 64-channel probe (left) or a linear 64-channel probe (right). (B) An example pair of functionally connected neurons in the MGB and A1. (i) Cross-correlograms (CCGs) of the spike trains of a neuronal pair for spontaneous activity (top) and stimulus-driven activity (bottom; DMR). CCGs with a peak crossing the threshold within 1-5 ms after MGB spikes were considered significant. The number of A1 spikes caused by MGB spikes was determined by the spikes within the 4ms window centered at the CCG peak, minus the spikes within each of the two 2ms windows flanking the 4ms central window. The synaptic transmission efficacy from the MGB neuron to the functionally connected A1 neuron was determined by the ratio of causal spikes and the total number of MGB spikes fired (in %). (ii) STRFs and spike waveforms of the MGB and A1 neurons in (i). (C) Efficacies derived from all pairs with significant CCGs for spontaneous (spon) and driven (stim) activity. Triangles: median (filled) and mean (open) of the distributions. (D) FR of functionally connected MGB and A1 neuron pairs under both spontaneous and stimulus-driven conditions. (MGB, p = 0.002; A1, p = 0.022; Wilcoxon signed-rank test). (E) The difference in best frequency (BF) between functionally connected MGB and A1 neurons. Only neuronal pairs with significant STRFs were included.
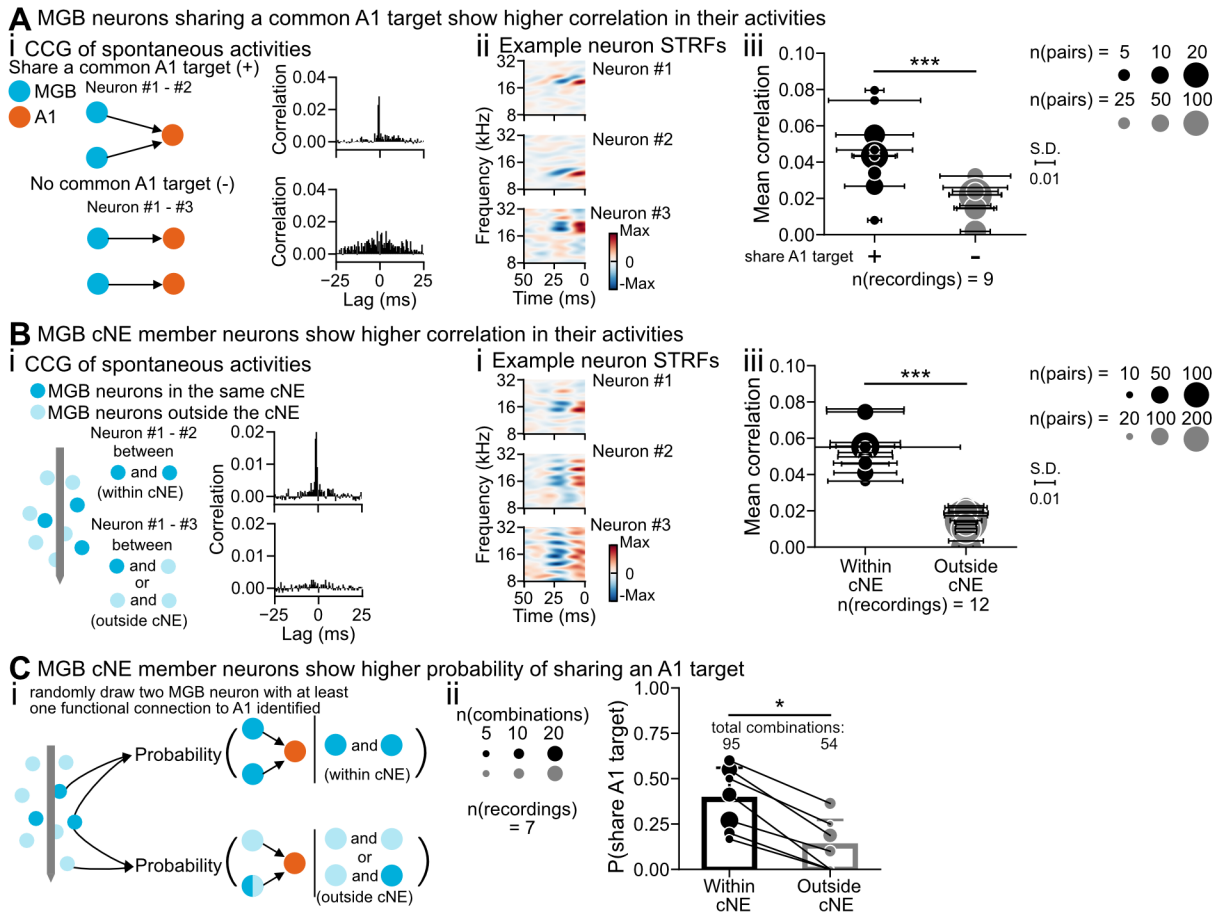
Figure 2.2

Figure 2.2 Groups of neurons with correlated spontaneous activities are identified as cNEs and are more likely to connect to the same A1 neuron. (A) Relationship between the correlation among MGB neurons and their connectivity to A1 neurons. (i) CCGs of spontaneous activities between MGB neurons #1 to #3. Top: Neurons #1 and #2 share a common A1 target; bottom: Neurons #1 and #3 do not share an A1 target. (ii) STRFs of the three example neurons in (i). (iii) The mean correlation among MGB neurons in each recording, considering whether they have a common A1 target (black dots) or not (gray dots). The size of the dots represents the number of MGB neuron pairs in each condition. Error bars show the S.D. of pairwise correlations in each recording. (F = 75.54, p = 7.0e-18, Nested ANOVA). (B) Correlation among MGB neurons based on their membership in a cNE. (i) Example CCGs. Neurons #1 and #2 belong to the same cNE (top), while neurons #1 and #3 are not members of the same cNE. (ii) STRFs of the three example neurons in (i). (iii) Mean correlation among MGB neurons residing within the same cNE (black dots) or not (gray dots) (F = 1377.75, p = 1.3e-240, Nested ANOVA). (C) Probability of MGB neurons sharing a target A1 neuron. (i) Schematics for calculating the connectivity probability. Neurons within the same cNE are dark blue; neurons outside the cNE are light blue. (ii) The probability of MGB neurons sharing a common A1 target, given whether they are in the same cNE (black dots) or not (gray dots) (p = 0.016, Wilcoxon signed-rank test). The size of the dots represents the number of unique combinations of MGB neuron pairs under each condition.

Figure 2.3

A Example MGB cNE with members connected to an A1 neuron

i MGB cNE

ii Locations of neurons on probes

iii CCG

B cNE spikes show higher efficacies at driving A1 neuron firing

i Raw spikes

ii Downsampled spikes

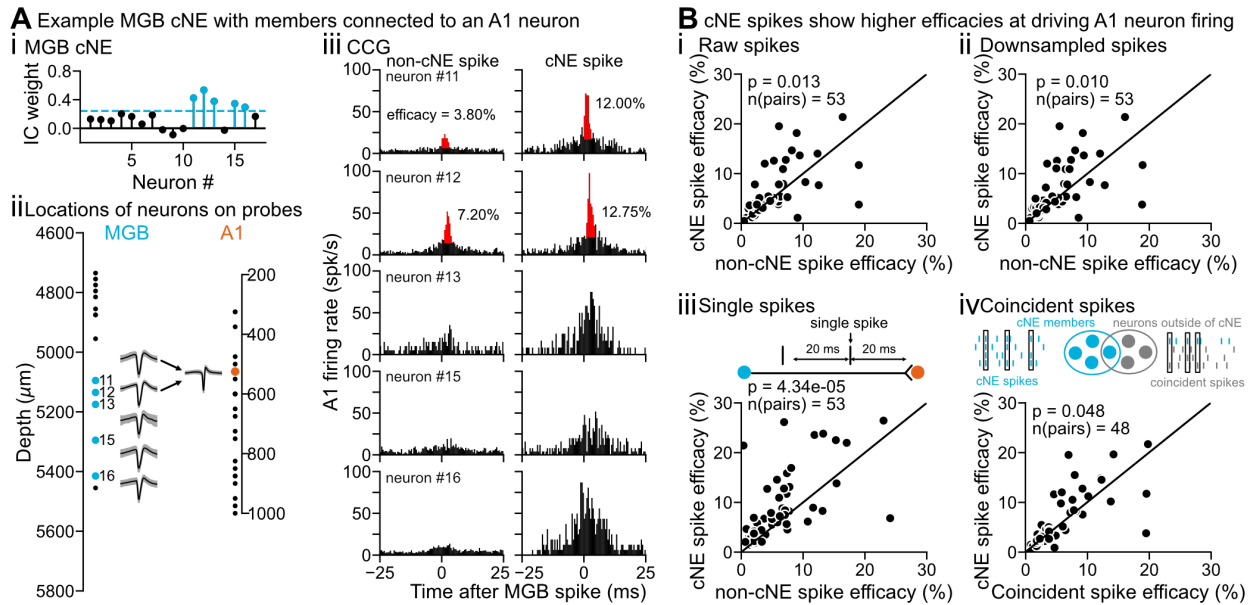**iii** Single spikes

iv Coincident spikes

Figure 2.3 cNE spikes show higher efficacy at driving A1 neuron firing. (A) An example MGB cNE with several members connected to the same A1 neuron. (i) IC weights of neurons in a recording. The dashed line represents the threshold for cNE membership; cNE members are labeled in blue. (ii) Depth and spike waveform of recorded neurons on the probes in the MGB (left) and A1 (right). Blue indicates the MGB cNE members shown in (i), while orange indicates the A1 neuron connected to two of the MGB cNE members. (iii) Left column: MGB-A1 CCGs for those MGB spikes that did not contribute to the cNE activity (non-cNE spikes). Causal spikes in significant CCGs are marked in red, and the corresponding efficacy is shown in the inset text. Right column: MGB-A1 CCGs for those MGB spikes that did contribute to the cNE activity (cNE spikes) (B) Efficacy of cNE spikes and non-cNE spikes from cNE member neurons based on spontaneous activities. (i) Efficacy calculated using raw spiking activities. (ii) Efficacy calculated after downsampling cNE spikes and non-cNE spikes to the same number. (iii) Efficacy calculated using only single spikes from the MGB neurons to eliminate effects from double spiking within ±20ms. (iv) Efficacy of cNE spikes versus coincident spikes, i.e., spikes where an MGB cNE neuron fired coincidentally with a random group of neurons matching the neuron count of the cNE (see Method for details). (Wilcoxon signed-rank test).
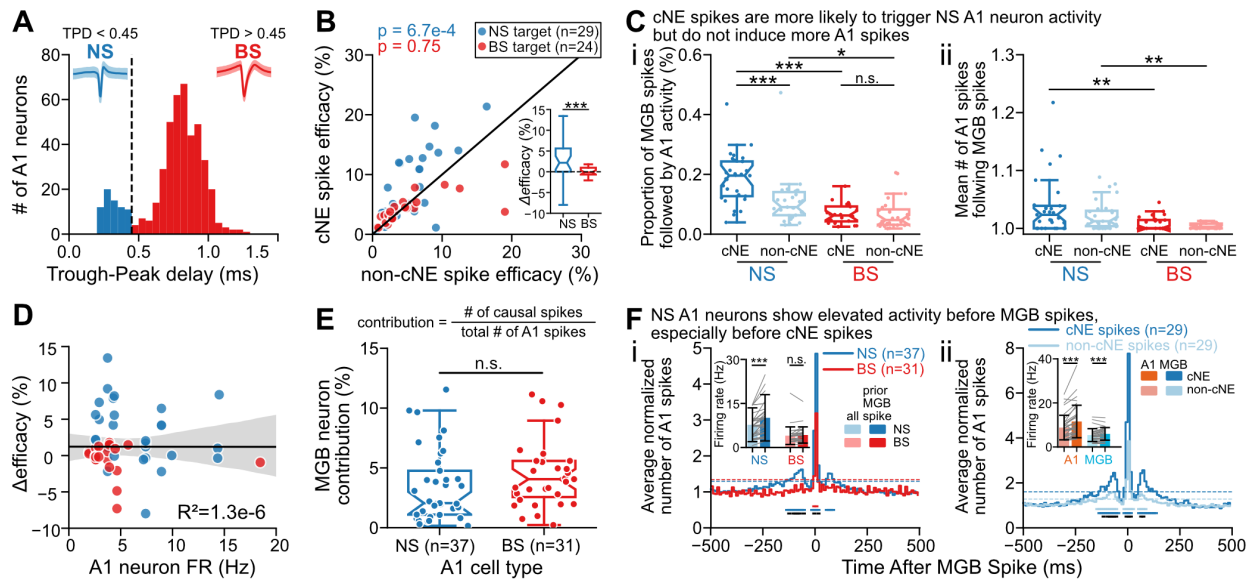
Figure 2.4

Figure 2.4 cNE spikes from MGB neurons exhibit higher efficacy for narrow-spiking A1 target neurons. (A) Classification of A1 neuron waveforms based on TPD, with the threshold distinguishing NS from BS neurons at 0.45 ms. (B) Efficacy of cNE spikes and non-cNE spikes from cNE member neurons when the A1 target neuron is NS (blue) or BS (red) (Wilcoxon signed-rank test). The inset shows the efficacy difference between cNE spikes and non-cNE spikes ($p = 7.5e-4$, Mann–Whitney U test). (C) Effect of MGB cNE spikes on A1 neuron firing. (i) Proportion of cNE and non-cNE spikes leading to spiking in the functionally connected A1 neuron within the causal window of 1-5ms for NS and BS A1 neurons (interaction, $F(1, 102) = 8.4$, $p = 0.005$; NS vs BS, $p = 1.7e-8$; cNE vs non-cNE, $p = 0.002$, two-way ANOVA; cNE vs non-cNE, NS: $p = 1.0e-7$, BS: $p = 1.0$, Wilcoxon signed-rank test; NS vs BS, cNE: $p = 6.6e-7$, non-cNE: $p = 0.013$, Mann–Whitney U test; with Bonferroni correction). (ii) Average number of A1 spikes following MGB spikes when at least one A1 spike was fired within the causal window. (interaction, $F(1, 102) = 0.98$, $p = 0.32$; NS vs BS, $p = 1.3e-4$; cNE vs non-cNE, $p = 0.075$, two-way ANOVA; NS vs BS, cNE: $p = 0.010$, non-cNE: 0.004, Mann–Whitney U test with Bonferroni correction). (D) Relationship between the efficacy change of cNE spikes relative to non-cNE spikes and the FR of the A1 target neuron. (E) Contribution of MGB spikes to A1 activity of NS or BS neurons ($p = 0.052$, Mann–Whitney U test). (F) Average A1 spike occurrence around MGB spikes, binned at 10ms. We normalized the A1 spike counts for each MGB-A1 neuronal pair to the mean level of baseline activity. The baseline activity levels were estimated using two 200 ms windows positioned 300ms away from MGB spikes. (i) NS (blue) and BS (red) A1 neuron activities around MGB spikes. Dashed lines indicate two standard deviations above the baseline activity. The red and blue lines indicate where the A1 neuron activity level is higher than the baseline level for BS and NS A1 neurons, respectively. The black lines indicate time ranges where the normalized number of spikes from NS A1 neurons is significantly higher than that from BS A1 neurons ($p < 0.05$, Mann-Whitney U test, with Bonferroni correction). Inset: firing rate of NS and BS A1 neurons within 200ms prior MGB spikes (dark) and during the entire recording (light) (NS, $p = 3.0e-9$; BS, $p = 0.08$, Wilcoxon signed-rank test). (ii) NS A1 neuron activities around cNE (dark blue) and non-cNE (light blue) MGB spikes. (Figure caption continued on the next page.)

(Figure caption continued from the previous page.) The dark blue and light blue lines indicate where NS A1 neuron activity level is higher than the baseline level around cNE and non-cNE MGB spikes, respectively. The black lines indicate time bins where the number of A1 spikes around cNE spikes are significantly higher than that around non-cNE spikes (p $<$0.01, Mann-Whitney U test, with Bonferroni correction). Inset: when the A1 target neuron is NS, the firing rate of A1 (orange) and MGB (blue) neurons within 200ms prior MGB cNE spikes (dark) and non-cNE spikes (light) (A1, p = 2.9e-7; MGB, p = 1.9e-4, Wilcoxon signed-rank test).
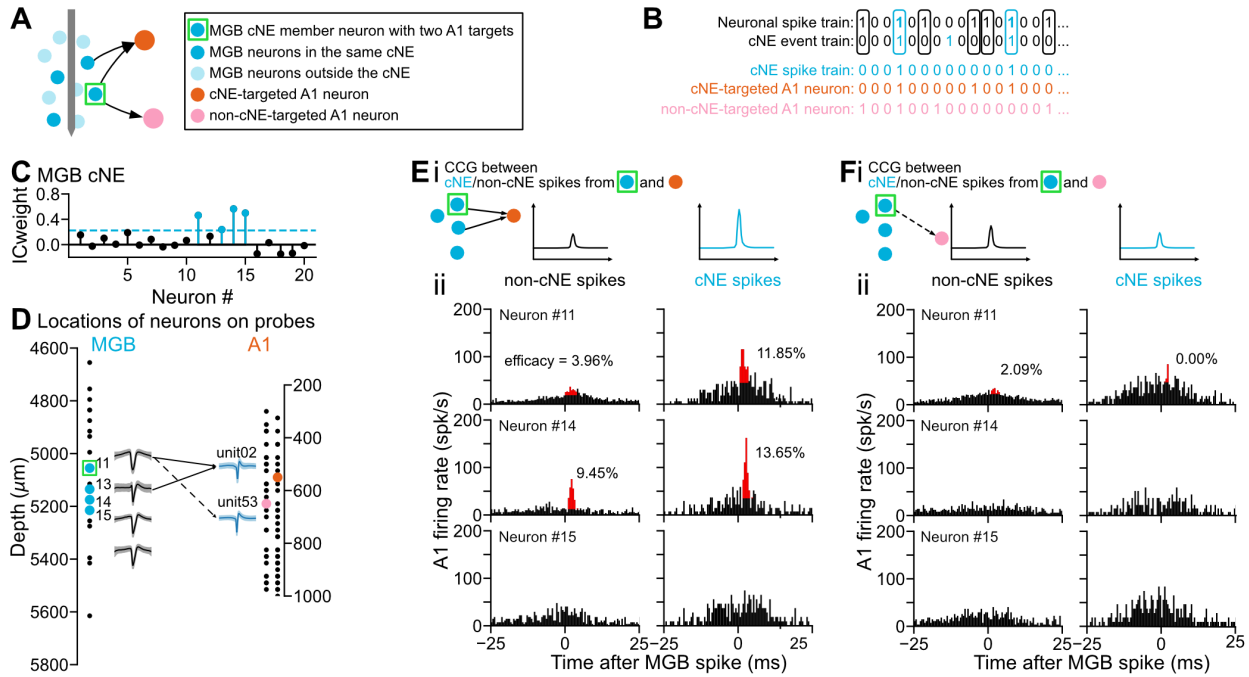
Figure 2.5

Figure 2.5 cNE spikes can have higher efficacy than non-cNE spikes at driving a cNE-targeted A1 neuron firing, although not a non-cNE-targeted A1 neuron. (A) Schematic depicting types of neurons in simultaneous recordings in the MGB and A1. "cNE-targeted A1 neuron" refers to A1 neurons that receive multiple inputs from an MGB cNE, while "non-cNE-targeted A1 neuron" refers to A1 neurons that receive input from only one member of the MGB cNE under examination. (B) Schematics illustrating the relationship of cNE/non-cNE spikes from an MGB neuron and the firing of cNE-targeted/non-cNE-targeted A1 neurons. (C) IC weights of MGB neurons in the example cNE. (D) Depth and spike waveform of recorded neurons in MGB (left) and A1 (right). Blue indicates cNE members, while orange and pink indicate cNE-targeted and non-cNE-targeted A1 neurons, respectively. (E) Efficacy of cNE and non-cNE spikes from members of an MGB cNE in driving the firing of a cNE-targeted A1 neuron. (i) Schematics illustrating the hypothesis that cNE spikes from an MGB neuron are more effective in driving firing of a cNE-targeted A1 neuron compared to non-cNE spikes. (ii) CCGs displaying the relationship between cNE/non-cNE spikes from cNE member neurons and a cNE-targeted A1 neuron. The inset numbers show the efficacy of cNE spikes and non-cNE spikes. (F) Efficacy of cNE and non-cNE spikes from members of the example MGB cNE shown in (E) in driving the firing of a non-cNE-targeted A1 neuron that nevertheless is connected to one of the cNE members, neuron #11. (i) Schematics illustrating the hypothesis that cNE spikes from an MGB neuron are not more effective in driving firing in a non-cNE-targeted A1 neuron compared to non-cNE spikes. (ii) CCGs displaying the relationship between cNE/non-cNE spikes from cNE member neurons and a non-cNE-targeted A1 neuron.
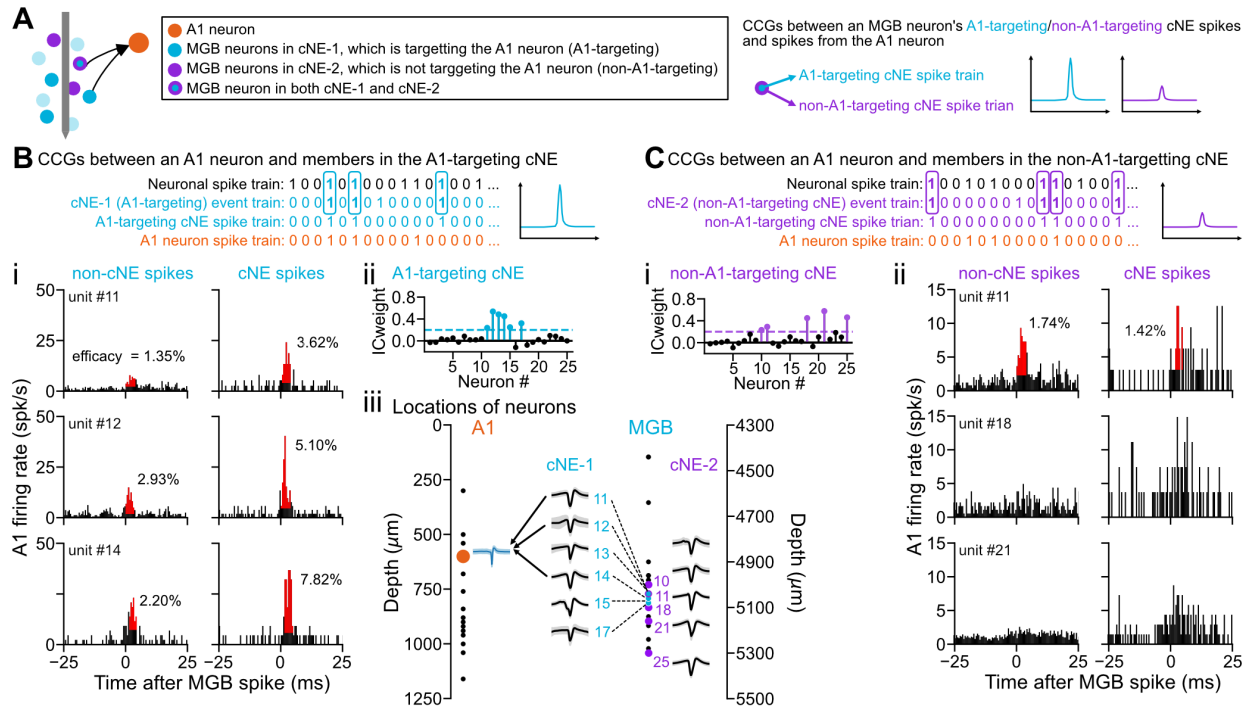
Figure 2.6

Figure 2.6 cNE spikes related to an A1-targeting cNE, but not a non-A1-targeting cNE, can show higher efficacy than non-cNE spikes. (A) Schematics of types of neurons in simultaneous recordings in the MGB that project to the same A1 neuron. "A1-targeting cNE" refers to MGB cNEs with multiple members connected to the A1 neuron (blue dots), while "non-A1-targeting cNE" refers to MGB cNEs with only one member connected to the A1 neuron (purple dots). We hypothesize that when an MGB neuron is a member of multiple cNEs (purple+blue dot), only cNE spikes related to the A1-targeting cNE (blue) will have higher efficacy in driving the A1 neuron firing, but not cNE spikes related to the non-A1-targeting cNE (purple). (B) cNE spikes from members of an A1-targeting cNE are more efficacious in driving the A1 neuron firing than non-cNE spikes. (i) CCGs displaying the relationship between cNE/non-cNE spikes from A1-targeting cNE members and the A1 neuron. The inset numbers show the efficacy of cNE spikes and non-cNE spikes. (ii) IC weights of MGB neurons in the example cNE. (iii) Depth and spike waveform of recorded neurons in MGB and A1. Blue indicates cNE members of the A1-targeting cNE and orange indicates the A1 neuron. (C) cNE spikes from members of a non-A1-targeting cNE are not more efficacious at driving the A1 neuron firing than non-cNE spikes. (i) IC weights of MGB neurons in the example cNE. (ii) Purple indicates cNE members of the non-A1-targeting cNE. (iii) CCGs displaying the relationship between cNE/non-cNE spikes from non-A1-targeting cNE members and the A1 neuron. One of the member neurons, neuron #11, is also a member of the cNE shown in (B).
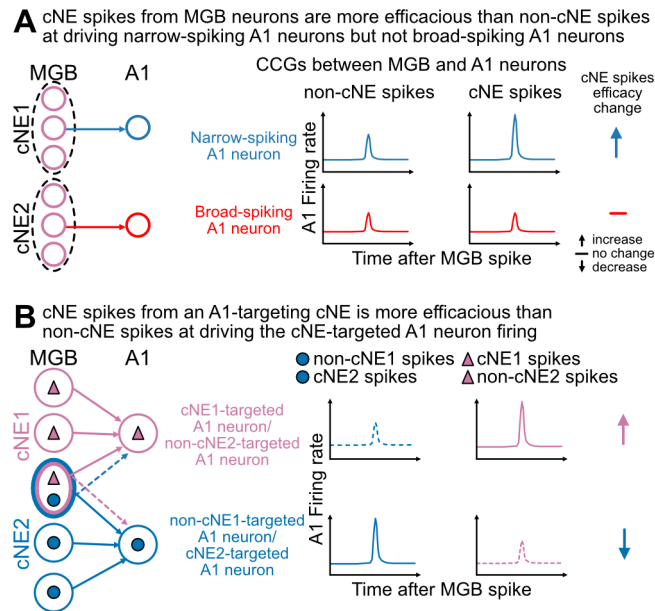
Figure 2.7

Figure 2.7 Summary of the specificity of cNE spikes from MGB neurons for A1 target neurons. (A) Comparison of the efficacy between cNE and non-cNE spikes when the A1 target neuron is BS or NS. When an MGB cNE member neuron is connected to a NS A1 neuron, the cNE spikes of the MGB neuron demonstrate higher efficacy than non-cNE spikes in driving the A1 neuron firing. Conversely, when an MGB cNE member neuron is connected to a BS A1 neuron, the cNE spikes of the MGB neuron do not exhibit higher efficacy than non cNE spikes. (B) cNE spikes associated with distinct cNEs from a shared MGB neuron exhibit varying efficacy in driving different A1 neuron firing. When an MGB neuron is member of two cNEs, cNE1 and cNE2, the cNE1 spikes from the neuron are more efficacious at driving firing in the cNE1-targeted A1 neuron compared to non-cNE1 spikes. However, the same cNE1 spikes, treated as non-cNE2 spikes, exhibit lower efficacy in driving firing in the cNE2-targeted A1 neuron.

Conclusions

Understanding of neural coordination requires knowledge in how coordinated activity is constructed from spike trains of individual neurons, what information is encoded, and how the information can be transmitted. In this study, we tackled these three aspects by simultaneously recording neural activities from the auditory thalamus and cortex and analyzing cNE activities in these regions.

Building upon prior research in the lab (See et al., 2018), we successfully identified cNEs in the auditory thalamus—an area that has received less attention in the investigation of coordinated neuronal activities. Similar to cNEs observed in the cortex, those identified in the thalamus also exhibited an enhanced capacity for coding stimulus information. Furthermore, cNEs in both regions displayed stability across both spontaneous and stimulus-driven activities, suggesting a structural foundation for cNE formation that is largely independent of specific stimuli. The discovery of cNEs in the auditory thalamus also provides evidence for cNEs as a ubiquitous organizational principle along the sensory pathway rather than being specific to cortical columns.

With simultaneous recordings in the MGB and A1, we successfully identified functionally connected neuronal pairs. Our findings confirm that cNEs enhance the efficacy of thalamocortical information transmission, as evidenced by the greater efficacy of MGB cNE spikes compared to non-cNE spikes in driving A1 neuron firing. Addressing these questions is crucial for unraveling the functional significance of cNEs in the auditory forebrain. While our work has provided answers to some initial inquiries, it has also paved the way for further investigation into the role of different types of neurons in cNE formation and function. Additionally, there are significant questions surrounding the modulation of cNE activity by behavioral states that warrant future exploration.

Methods

Animals All experimental procedures were approved by the Institutional Animal Care and Use Committee at the University of California, San Francisco (UCSF), and followed the guidelines of the National Institute of Health for the care and use of laboratory animals. Thirty-three female Sprague-Dawley rats (wild type, 250-350g, 2-4 months; RRID: MGI: 5651135), sourced from Charles River, were used in this study.

Surgery The detailed procedures were as described in previous studies (See et al., 2018; Homma et al., 2020). Briefly, anesthesia was induced with a combination of ketamine (100 mg/kg, Ketathesia, HenrySchein) and xylazine (3.33 mg/kg, AnaSed, Akorn), along with atropine (0.54 mg/kg, AtroJectSA, HenrySchein), dexamethasone (4 mg/kg, Dexium-SP, Bimeda), and meloxicam (2 mg/kg, Eloxiject, HenrySchein). Additional doses of ketamine (10-50 mg/kg) and xylazine (0-20 mg/kg) were given as needed to maintain anesthesia. Local anesthesia was provided using lidocaine (Lidoject, 2%, HenrySchein) prior to making incisions. The respiratory rate, heart rate, and depth of anesthesia were continuously monitored, and anesthesia was adjusted as needed. The body temperature was monitored and maintained at 37°C using a homeothermic blanket system (Harvard Apparatus 55-7020). Lubricant ophthalmic ointment (Artificial Tears, HenrySchein) was applied to protect the eyes. A tracheotomy was performed to ensure stable breathing during recording. To access the brain, the skin, muscle, skull, and dura over the right temporal lobe were removed, and silicone oil (Sigma-Alderich) was applied to cover the cortex. A bone rongeur was used to widen the craniotomy window and provide dorsal access to the MGB. A cisternal drain was performed to prevent brain swelling.

Electrophysiology The frequency organization of auditory cortex was first mapped using Tungsten electrodes. A1 was identified as the area with a high to low frequency preference gradient on the rostral-causal axis and short latency response to pure tones (Polley et al., 2007). Subsequently, we conducted electrophysiological recordings in two areas simultaneously (Figure

1A): the MGB by using a linear silicon probe with 64 channels (H3, 20μm channel spacing, Cambridge NeuroTech), and A1 by using either a 2-shank probe with 64 channels (H2, 25μm channel spacing, Cambridge NeuroTech) or a linear silicon probe with 64 channels (H3). The ventral division of the MGB is characterized by a low to high frequency gradient on the dorsal-ventral axis (Morel et al., 1987; Anderson and Linden, 2011). The probes were inserted using microdrives (David Kopf Instruments) at a rate of 25 μm/s to a depth of 4500 to 6000 μm from the surface of the cortex to reach MGB (Figure 1.1A) and 900 to 1300 μm in A1 along the columnar structure (Figure 1.7A), respectively. Extracellular voltage traces were recorded at a sampling rate of 20 kHz with an Intan RHD2132 Amplifier system (Intan Technologies). MU activities (Figure 1.1A and 1.7A) were defined as negative peaks crossing 4 standard deviations from the mean in the extracellular voltage trace filtered between 300 and 6000 Hz. Single unit activities were obtained by spike sorting using Kilosort 2.5 (Steinmetz et al., 2021; Pachitariu et al., 2023), followed by manual curation using Phy (https://github.com/cortex-lab/phy). In the manual curation process, we visually evaluated individual clusters by examining auto-correlograms, spike waveforms, the stability of spike amplitude over time, the persistence of activity over time, the cluster's separation from noise in the feature space, and other visual aids provided by phy2 for distinguishing single-unit clusters from multi-unit or noise clusters. Subsequently, the identified units underwent filtering based on specific criteria: inter-spike interval (ISI) violation within 2ms $<1.5\%$. The majority of single units exhibited an ISI violation lower than 0.25%; peak signal-to-noise ratio (SNR) of the waveform >1.5 (median peak SNR: MGB: 4.52, A1: 3.77); and firing rates >0.1 Hz to eliminate potential multi-units. To assess the reliability of activity of the single units across the entire recording duration we obtained the presence ratio. This is the ratio of the number of blocks where the unit showed activity and the total number of blocks in a recording session. To calculate the presence ratio, the entire recording was divided into 100 equal time blocks. The majority of the obtained single units were active in more than 95% of the time blocks. This sorting resulted in single units that exhibit low ISI violations, high peak SNR, firing rates with a log-normal distribution, and a more consistent

56

presence during recording when compared to all clusters generated by Kilosort. To identify oscillatory response in MGB or A1, single units on the same electrode were combined to form multi-units (Figure 1.8).

Stimuli To measure frequency tuning, we presented pure tones with frequencies ranging from 0.5 to 32 kHz in 0.13 octave steps and sound levels from 0 to 70 dB in 5 dB steps (50ms, 5ms ramps). Each frequency-sound level combination was presented once in a pseudo-random order, with an inter-stimulus interval of 250ms. To assess STRFs, we used a 15-minute dynamic moving ripple (DMR) (Escabí and Schreiner, 2002). The DMR consisted of 40 sinusoidal carrier frequencies per octave in the range of 0.5 to 40 kHz, each with a random phase. The carriers were slowly modulated (maximum rate of change $\leq$ 3Hz) by a spectrotemporal envelope with a maximum spectral modulation rate of 4 cycles/octave, a maximum temporal modulation rate of 40 cycles/s, and a maximum modulation depth of 40 dB. The mean intensity of the DMR was set at 70 dB sound pressure level. We selected DMR as the stimulus for analyzing cNEs' response to sound stimuli, as overt onset response effects for the 15-minute continuous stimulus is negligible. Additionally, DMR has been observed to reduce oscillatory states in the neural population (Miller and Schreiner, 2000). All auditory stimuli were generated using MATLAB (MathWorks) and calibrated using a 1/2-inch pressure field microphone (Type 4192, Bruel and Kjær). The stimuli were delivered contralaterally from the recording site using a closed-field electrostatic speaker (EC1, TuckerDavis Technologies) at a sampling rate of 96 kHz.

Detecting cNEs To identify groups of neurons that exhibit synchronized co-activation, referred to as "cNEs", we used a method combining PCA and ICA (Lopes-dos Santos et al., 2013; See et al., 2018). We selected a bin size of 10ms as a standard synchronization span because it represents the most appropriate time window to capture the synaptic integration window of most cortical neurons (Léger et al., 2005; D'amour and Froemke, 2015). First, the individual spike trains of simultaneously recorded neurons were binned and z-scored. Next, the z-scored spike matrix underwent PCA to obtain the eigenvalues of the spike train correlation matrix. To determine the

number of cNEs, we took eigenvalues to be significant if their value exceeded the 99.5th percentile of the Marchenko-Pastur distribution, which describes the probability density function of eigenvalues of large rectangular random matrices (Marčenko and Pastur, 1967; See et al., 2018) (Figure 1.2A-ii). We then performed ICA (FastICA) on the subspace spanned by the eigenvectors corresponding to the significant eigenvalues. The resulting ICs represent groups of neurons with shared spiking events. The weight of each neuron on an IC indicates the neuron's contributions to the cNE (Figure 1.2A-iii). As the signs of IC weights were arbitrary, for each IC, the direction with the largest absolute weight was rendered positive. The length of each IC was normalized to one, making an IC with equal contribution from all neurons have weights of $1/\sqrt{N}$, where N was the number of neurons in the recording. Neurons with weights over $1/\sqrt{N}$ were referred to as "cNE members" (Oberto et al., 2022) (Figure 1.2A-iv).

The strength of the cNE activation at each time point was measured by the similarity between the activity of cNE members as well as the cNE pattern, i.e., which neurons in a penetration were cNE members. The similarity can be measured as the square of the weighted sum of the z-scored spike counts, $s = z^T w w^T z = z^T P z$, where z is the z-scored spike counts of cNE members at each time point, w is the IC weights of cNE members, and the projection matrix P is the outer product of w. To consider only co-activation of multiple cNE members, we set the diagonal of the projection matrix to zero and obtained the modified projection matrix P^*. cNE activity strength was calculated as $s = z^T P^* z$. A null distribution of cNE activity was obtained by projecting a circularly shifted spike matrix, where the temporal relationship of neurons was disrupted, to the template matrix (See et al., 2018). This process was iterated 50 times, and the threshold of cNE activation was defined as the 99.5th percentile of the null distribution (Figure 1.2A-v). The spikes of cNE members within the selected time bin where the cNE was active were referred to as "cNE spikes".

Matching cNEs across different bin sizes We used the correlation between IC weights of all neurons in a penetration to assess the similarity of cNE patterns across different synchronization

windows (i.e., time bin width: 2, 5, 10, 20, 40, 80 and 160ms). To visualize the similarity of cNEs identified using 10ms bins to those identified using other bin sizes, we calculated the cNEs for the same recording using other bin sizes. We displayed the cNEs whose IC weights were best correlated with the 10ms cNE (Figure 1.3A). To measure the variability of cNE identities across bin sizes (Figure 1.3B and C), we matched each cNE to the most similar cNE calculated using reference bins (i.e., when using 10ms as the reference bin size, to the 10ms cNE which had the best-correlated IC weights). The proportion of shared members with a reference cNE was then calculated by dividing the number of members in a cNE that were also identified as members in its matching reference cNE by the total number of unique members in both cNEs combined.

The significance of the match was determined based on the null distribution of IC weight correlations between matched cNEs. For example, to determine the significance of the correlation between the IC weights of a 10ms cNE with its most correlated 160ms cNE, we first generated a null distribution of IC weight correlations. We circularly shifted spike trains and then applied PCA/ICA to identify sham cNEs using the shuffled spike matrices binned at 160ms, maintaining the same number of cNEs as the original 160ms cNEs. Then we identified the most correlated sham 160ms cNE for the 10ms cNE. This process was repeated 1000 times to generate the null distribution of correlation values. The significance threshold was set at p $<$0.01.

Assessing stability of cNEs To assess the stability of cNEs during and across spontaneous and stimulus-driven activity, we compared the cNEs from adjacent recording segments (Figure 1.4A). To match the IC weights of cNEs identified from the different recording segments, we used an iterative process that involved selecting cNE pairs from the two segments with the highest correlations (Spearman's r) Oberto et al. (2022). First, we computed the correlations between all possible pairs of cNEs that were generated from the two segments. Then, the pair with the highest correlation was set aside, and the same process was repeated with the remaining cNEs until all cNEs were paired. If there were any remaining cNEs that did not have a match due to a difference in the number of cNEs between the two segments, they were left unmatched.

To generate a null distribution of IC weight correlations between matched cNEs from two recording segments (Figure 1.4D), we circularly shifted spike trains within each activity block. We then applied PCA/ICA to identify sham cNEs using the resulting shuffled spike matrices. As the shuffling disrupted correlations between neurons, very few eigenvalues exceeded the upper bounds of the Marchenko-Pastur distribution. To address this, we maintained the number of sham cNEs in the shuffled data equivalent to the number of significant eigenvalues obtained from the original spike matrix. The sham cNEs from adjacent activity blocks were then matched following the procedure described above. This iterative process was repeated 1000 times to establish a null distribution of IC weight correlations for the matched cNEs. The 99.5th percentile of each null distribution was set as the significance threshold.

False positive detection of cNEs To assess the potential for false positive cNE detection, we applied the cNE detection algorithm to shuffled data, using the same criteria as those applied to the real dataset. This process was repeated 10 times, resulting in an average count of false positive cNEs across the circularly shifted data (Figure 1.4F). Despite conducting 10 iterations, false positive cNEs were not consistently identified in neighboring blocks. In cases where a false positive cNE was detected (for example, when an eigenvalue computed from shuffled data exceeded the Marchenko-Pastur distribution), we evaluated its stability by measuring the highest correlation of its IC weights with those of real cNEs in the adjacent block (Figure 1.4E). The significance of false positive cNE IC weight correlations was determined using the same threshold established for real cNEs.

STRF analysis For analysis, we down-sampled DMR to a resolution of 0.1 octaves in frequency and 5ms in time. We used the reverse correlation method to obtain the STRFs of the units (Theunissen et al., 2000; Escabí and Schreiner, 2002). To derive the STRFs, we averaged the spectrotemporal envelopes of the stimulus over a period of 100ms preceding spikes (Figure 1.1B and 1.6A). Positive (red) values on a STRF indicate that the sound energy at that frequency and time tends to increase the firing rate of the unit, while negative (blue) values indicate where the

stimulus tends to decrease the firing rate of the unit. The BF and response latency of the unit were determined by the frequency and latency associated with the highest absolute value in the STRF (Miller et al., 2002). We also determined the PTD as a measure of STRF strength.

A STRF was considered significant if it reliably described a neuron's response to DMR sound. To assess the reliability of a STRF, we divided a neuron's spikes into two equal halves and generated two corresponding STRFs (STRF A and B) using each half (Qiu et al., 2003). The similarity between STRF A and B was computed using Pearson's correlation. This process was reiterated 1000 times, and the average STRF similarity across these iterations was used as the measure of reliability. To determine the statistical significance of a STRF's reliability, we constructed a null distribution by reversing the neuron's spike train, thus disrupting the temporal correlation of neural responses to the stimulus. We considered STRFs with a reliability surpassing a z-score of 2.58 to be significant.

We used MI as the metric to quantify the amount of information we can obtain about the stimulus by observing spikes of neurons or cNEs (Atencio et al., 2008; See et al., 2018). The stimulus segments preceding each spike was projected onto the STRF via the inner product $z = s * STRF$. The projection values were then binned to get the probability distribution $P(z|spike)$. The *a priori* distribution of stimulus projection values, $P(z)$, was calculated by projecting all stimulus segments of DMR onto the STRF, regardless of spike occurrence. Both distributions $P(z)$ and $P(z|spike)$ were normalized relative to the mean μ and standard deviation σ of $P(z)$, by $x = ((z - \mu))/\sigma$, resulting in $P(x)$ and $P(x|spike)$. The MI between STRF projection values and single spikes was computed according to $I = \int dx P(x|spike) log_2 \frac{P(x|spike)}{P(x)}$.

STRF comparisons between cNEs and non-cNE groups of neurons To control for the potential influence of population synchrony on a cNE due to independent neuron activity, we compared STRFs derived from cNEs and non-cNE groups of neurons. If less than half of members had significant STRFs, the cNE was excluded from analysis.

First, we compared the group STRFs of cNEs and non-cNE groups of neurons (Figure 1.6B-ii and C-ii) (See et al., 2018). The group STRF was calculated using all spikes from neurons within a group. To generate non-cNE groups of neurons relative to a cNE, we first selected one neuron from the cNE and then sampled from the remaining neurons with significant STRFs within a penetration, forming a group with the same number of neurons as the cNE for comparison. This process excluded other member neurons of the cNE. This procedure was repeated for all members of the cNE, generating all possible combinations of neurons, each including exactly one member neuron from the cNE under examination. Combinations of neurons that included more than one neuron from any other cNEs in the same recording were then also excluded. For each cNE/non-cNE group comparison, we subsampled the spikes in the cNE and the non-cNE groups to the same number. Subsequently, STRF PTD and MI of the cNE group were compared to the median values of the non-cNE groups.

We also compared the STRFs of cNE spikes with those of coincident spikes from a single neuron (Figure 1.6B-iii and C-iii) to assess the influence of random coincidence on stimulus preference. To obtain coincident spikes from a specific neuron, we first sampled neurons from the recorded population that do not share membership with the neuron under examination in any cNE to create a non-cNE group. We kept the number of neurons in the non-cNE group the same as the cNE to which the neuron being examined belongs. This sampling process was restricted to neurons exhibiting significant STRFs. The coincident spikes of the cNE member refer to spikes within 10ms of spikes from other neurons within the non-cNE group. We repeated this procedure to generate all possible combinations of non-cNE groups, each containing the cNE member and excluding any neuron that shares membership with the neuron under scrutiny. Coincident spike trains with less than 100 events were discarded. For each cNE spike/non-cNE spike comparison, we subsampled the cNE spikes and spikes from the non-cNE groups to the same number. Subsequently, the cNE spike STRF PTD and MI were compared to the median values of the random spike STRF PTD and MI from the non-cNE groups.

Quantifying slow oscillations in neural activity To determine whether the neural activity in a recording showed a prominent pattern of slow oscillations, we measured silence density and the CV of MU firing rate. Silence density was defined as the fraction of 20ms time bins with no population activity (zero spikes) (Mochol et al., 2015). The CV of MU firing rate was calculated as $CV = \sigma/\mu$, where μ is the mean firing rate and σ is the standard deviation of the firing rate binned at 20ms time bins.

Detecting Functional Connectivity The precise temporal correlations between spike trains can provide insights into the functional connectivity between neurons (Perkel et al., 1967; Senzai et al., 2019). Putative excitatory connections can be identified by deviations from the baseline in the CCG at short time-lags (1-5ms) (Figure 2.1B-i). To estimate the baseline firing rate, CCGs binned at 0.5ms windows were convolved with a Gaussian window (sigma=7ms). The statistical threshold for detecting a significant deviation from the baseline at each time bin was set at the 99.9th percentile of a Poisson distribution based on the baseline rate. We considered a putative connection to be significant when at least two consecutive time bins in the CCG crossed the threshold within the causal window of 1-5ms after MGB spikes. To avoid the confound of stimulus-induced correlated firing, only spontaneous activities were used to determine the functional connectivity between neurons. The efficacy of a thalamic neuron or cNE in driving the response of a connected cortical neuron was measured as the number of MGB spikes causal to cortical spikes divided by the total number of thalamic spikes (Alonso et al., 1996). The contribution of the MGB to cortical response was measured as the number of causal MGB spikes divided by the total number of spikes in the A1 neuron.

Estimating the probability of two MGB neurons sharing an A1 target To investigate the relationship between the cNE membership of MGB neurons and their connectivity to A1 neurons, we estimated the probability of two MGB neurons sharing a common A1 target in each recording, depending on whether the two neurons were part of the same cNE (Figure 2.2C). This analysis only considered MGB neurons with identified A1 targets. We included recordings that had a

minimum of 5 such MGB neurons and at least one pair of MGB neurons sharing an A1 target (7 out of 12 recordings). For any randomly drawn pair of MGB neurons, four potential outcomes were possible, depending on whether the two neurons were members of the same cNE and if they were connected to the same A1 neuron. The probability of two MGB neurons of the same cNE sharing an A1 target was calculated as the number of pairs in the same cNE and sharing an A1 target divided by the total number of pairs in the same cNE. Similarly, the probability of a pair of neurons sharing an A1 target when they are not members of the same cNE was calculated as the number of pairs not in the same cNE and sharing an A1 target divided by the total number of pairs not in the same cNE.

Comparing the efficacy of cNE spikes and coincident spikes To control for the potential influence of population effect arising from independent neural activity, we compared the efficacy of cNE spikes from a given neuron with that of coincident spikes from a group of neurons that are not members of the cNE, termed a non-cNE group. To construct non-cNE groups for an MGB neuron, we sampled neurons from the recorded population that did not share membership of any cNE. The number of neurons in the non-cNE group matched the size of the cNE to which the examined neuron belonged. Coincident spikes of the cNE member referred to spikes within 10ms of spikes from other neurons within the non-cNE group. This process was repeated to generate all possible combinations of non-cNE groups, with coincident spike trains containing fewer than 100 events discarded. Subsequently, both the cNE spike train and all coincident spike trains were subsampled to the same number of events. We then compared the average efficacy of cNE spikes and coincident spikes based on calculations from 10 different subsamplings.

Permutation test We used permutation tests to determine the statistical significance of differences in CCGs among neurons based on their membership (Figure 1.2C and 1.3D), as well as to assess differences in the proportion of stable cNEs between different stimulus conditions (Figure 1.4E and 1.7E). For example, to assess the difference in CCGs between member pairs and non-member pairs (Figure 1.2C), we shuffled the membership labels of the CCGs and calculated the difference

64

between the average CCGs of member and non-member pairs. We repeated this process 10,000 times to generate null distributions of the CCG difference for each data point. The 0.5th and 99.5th percentiles of the null distribution were taken as the cutoffs for significance. We considered consecutive time bins around 0ms-lag with $p < 0.01$ to be significant. To assess the difference in the proportion of stable cNEs, we shuffled the stimulus condition label (spontaneous ['spon'], DMR ['dmr'], or cross condition comparison ['cross']) and repeated this process 10,000 times to generate a null distribution of the difference in proportion. The significance level was then determined based on the null distribution.

Statistics Statistical analyses were performed in Python. To compare two unpaired groups (e.g., Figure 1.2B), we used Mann–Whitney U tests. To compare two paired groups (e.g., Figure 1.4F), we used Wilcoxon signed-rank tests. To compare two groups while accounting for variability within subgroups (e.g., Figure 2.2A-iii), we used Nested ANOVA. To determine the effect of two variables (e.g., Figure 2.4E), we used two-way ANOVA with *post hoc* rank tests and Bonferroni correction. Permutation tests (e.g., Figure 1.2C), and Monte Carlo methods (e.g., Figure 1.4D) were used as described above. To determine if two samples are drawn from the same distribution, we used Kolmogorov-Smirnov test (Figure 1.3D). The specific applications of these tests are explained in the results section and figure legends. Significance levels are noted as n.s. ($p \geq 0.05$), * ($p < 0.05$), ** ($p < 0.01$) and *** ($p < 0.001$).

References

Abbott LF, Dayan P (1999) The effect of correlated variability on the accuracy of a population code. *Neural computation* 11:91–101. 20

Alonso JM, Usrey WM, Reid RC (1996) Precisely correlated firing in cells of the lateral geniculate nucleus. *Nature* 383:815–819. 1, 2, 32, 63

Anderson L, Wallace M, Palmer A (2007) Identification of subdivisions in the medial geniculate body of the guinea pig. *Hearing research* 228:156–167. 31

Anderson LA, Linden JF (2011) Physiological differences between histologically defined subdivisions in the mouse auditory thalamus. *Hearing Research* 274:48–60. 56

Aschauer DF, Eppler JB, Ewig L, Chambers AR, Pokorny C, Kaschube M, Rumpel S (2022) Learning-induced biases in the ongoing dynamics of sensory representations predict stimulus generalization. *Cell reports* 38. 16

Atencio CA, Schreiner CE (2010) Laminar diversity of dynamic sound processing in cat primary auditory cortex. *Journal of neurophysiology* 103:192–205. 13

Atencio CA, Schreiner CE (2013) Auditory cortical local subnetworks are characterized by sharply synchronous activity. *Journal of Neuroscience* 33:18503–18514. 5, 6, 12, 17

Atencio CA, Sharpee TO, Schreiner CE (2008) Cooperative Nonlinearities in Auditory Cortical Neurons. *Neuron* 58:956–966. 37, 61

Averbeck BB, Latham PE, Pouget A (2006) Neural correlations, population coding and computation. *Nature reviews neuroscience* 7:358–366. 31

Baeg E, Kim Y, Huh K, Mook-Jung I, Kim H, Jung M (2003) Dynamics of population code for working memory in the prefrontal cortex. *Neuron* 40:177–188. 4, 42

Barthó P, Hirase H, Monconduit L, Zugaro M, Harris KD, Buzsaki G (2004) Characterization of neocortical principal cells and interneurons by network interactions and extracellular features. *Journal of neurophysiology* 92:600–608. 37

Bartlett EL (2013) The organization and physiology of the auditory thalamus and its role in processing acoustic features important for speech perception. *Brain and language* 126:29–48. 5

Bartlett EL, Wang X (2007) Neural representations of temporally modulated signals in the auditory thalamus of awake primates. *Journal of neurophysiology* 97:1005–1017. 5, 17, 44

Bathellier B, Ushakova L, Rumpel S (2012) Discrete neocortical dynamics predict behavioral categorization of sounds. *Neuron* 76:435–449. 4, 5, 31, 42

Bizley JK, Walker KM, King AJ, Schnupp JW (2010) Neural ensemble codes for stimulus periodicity in auditory cortex. *Journal of Neuroscience* 30:5078–5091. 4, 7, 42

Boucly CJ, Pompili MN, Todorova R, Leroux EM, Wiener SI, Zugaro M (2022) Flexible communication between cell assemblies and 'reader' neurons. *bioRxiv* pp. 2022–09. 4, 42, 43

Braitenberg V, Schutz A (1991) Anatomy of the cortex: studies of brain function. 31

Brandner S, Redies H (1990) The projection from medial geniculate to field ai in cat: organization in the isofrequency dimension. *Journal of Neuroscience* 10:50–61. 44

Briggs F, Usrey MW (2007) Cortical activity influences geniculocortical spike efficacy in the macaque monkey. *Frontiers in Integrative Neuroscience* 1:63. 39, 43

Brosch M, Schreiner CE (1999) Correlations between neural discharges are related to receptive field properties in cat primary auditory cortex. *European Journal of Neuroscience* 11:3517–3530. 5, 6

Bruno RM, Sakmann B (2006) Cortex is driven by weak but synchronously active thalamocortical synapses. *Science* 312:1622–1627. 32, 34

Buzsáki G (2010) Neural Syntax: Cell Assemblies, Synapsembles, and Readers. *Neuron* 68:362–385. 4, 7, 8, 17, 31

Cariani P, Baker JM (2022) Time is of the essence: Neural codes, synchronies, oscillations, architectures. *Frontiers in Computational Neuroscience* 16:898829. 40

Carrillo-Reid L, Miller JEK, Hamm JP, Jackson J, Yuste R (2015) Endogenous sequential cortical activity evoked by visual stimuli. *Journal of Neuroscience* 35:8813–8828. 7

Chamberland S, Yang HH, Pan MM, Evans SW, Guan S, Chavarha M, Yang Y, Salesse C, Wu H, Wu JC et al. (2017) Fast two-photon imaging of subcellular voltage dynamics in neuronal tissue with genetically encoded indicators. *elife* 6:e25690. 5

Chase SM, Young ED (2008) Cues for sound localization are encoded in multiple aspects of spike trains in the inferior colliculus. *Journal of neurophysiology* 99:1672–1682. 40

Chauvette S, Crochet S, Volgushev M, Timofeev I (2011) Properties of slow oscillation during slow-wave sleep and anesthesia in cats. *Journal of Neuroscience* 31:14998–15008. 14, 21

Clay Reid R, Alonso JM (1995) Specificity of monosynaptic connections from thalamus to visual cortex. *Nature* 378:281–284. 33, 34

Connors BW, Gutnick MJ (1990) Intrinsic firing patterns of diverse neocortical neurons. *Trends in neurosciences* 13:99–104. 37, 38

Contreras D, Timofeev I, Steriade M (1996) Mechanisms of long-lasting hyperpolarizations underlying slow sleep oscillations in cat corticothalamic networks. *The Journal of physiology* 494:251–264. 14

Cowan RL, Wilson CJ (1994) Spontaneous firing patterns and axonal projections of single corticostriatal neurons in the rat medial agranular cortex. *Journal of neurophysiology* 71:17–32. 15

Dan Y, Alonso JM, Usrey WM, Reid RC (1998) Coding of visual information by precisely correlated spikes in the lateral geniculate nucleus. *Nature neuroscience* 1:501–507. 12

Dantzker J, Callaway E (2000) Laminar sources of synaptic input to cortical inhibitory interneurons and pyramidal neurons. *Nature neuroscience* 3:701–707. 37

Dasilva M, Camassa A, Navarro-Guzman A, Pazienti A, Perez-Mendez L, Zamora-López G, Mattia M, Sanchez-Vives MV (2021) Modulation of cortical slow oscillations and complexity across anesthesia levels. *Neuroimage* 224:117415. 21

de Venecia RK, McMullen NT (1994) Single thalamocortical axons diverge to multiple patches in neonatal auditory cortex. *Developmental brain research* 81:135–142. 44

deCharms RC (1998) Information coding in the cortex by independent or coordinated populations. *Proceedings of the National Academy of Sciences* 95:15166–15168. 20

Decharms RC, Merzenich MM (1996) Primary cortical representation of sounds by the coordination of action-potential timing. *Nature* 381:610–613. 1, 4

DeNardo LA, Liu CD, Allen WE, Adams EL, Friedmann D, Fu L, Guenthner CJ, Tessier-Lavigne M, Luo L (2019) Temporal evolution of cortical ensembles promoting remote memory retrieval. *Nature neuroscience* 22:460–469. 31

Domanski AP, Kucewicz MT, Russo E, Tricklebank MD, Robinson ES, Durstewitz D, Jones MW (2023) Distinct hippocampal-prefrontal neural assemblies coordinate memory encoding, maintenance, and recall. *Current Biology* 33:1220–1236. 4, 42

D'amour JA, Froemke RC (2015) Inhibitory and excitatory spike-timing-dependent plasticity in the auditory cortex. *Neuron* 86:514–528. 35, 57

Ebrahimi S, Lecoq J, Rumyantsev O, Tasci T, Zhang Y, Irimia C, Li J, Ganguli S, Schnitzer MJ (2022) Emergent reliability in sensory cortical coding and inter-area communication. *Nature* 605:713–721. 4

Eggermont JJ (2000) Sound-induced synchronization of neural activity between and within three auditory cortical areas. *Journal of Neurophysiology* 83:2708–2722. 5, 6

El-Gaby M, Reeve HM, Lopes-dos Santos V, Campo-Urriza N, Perestenko PV, Morley A, Strickland LA, Lukács IP, Paulsen O, Dupret D (2021) An emergent neural coactivity code for dynamic memory. *Nature Neuroscience* 24. 18

Escabí MA, Schreiner CE (2002) Nonlinear Spectrotemporal Sound Analysis by Neurons in the Auditory Midbrain. *Journal of Neuroscience* 22:4114–4131. 6, 57, 60

Feldmeyer D, Qi G, Emmenegger V, Staiger JF (2018) Inhibitory interneurons and their circuit motifs in the many layers of the barrel cortex. *Neuroscience* 368:132–151. 37

Filipchuk A, Schwenkgrub J, Destexhe A, Bathellier B (2022) Awake perception is associated with dedicated neuronal assemblies in the cerebral cortex. *Nature Neuroscience* 25:1327–1338. 10, 18

Geiger JR, Melcher T, Koh DS, Sakmann B, Seeburg PH, Jonas P, Monyer H (1995) Relative abundance of subunit mrnas determines gating and ca2+ permeability of ampa receptors in principal neurons and interneurons in rat cns. *Neuron* 15:193–204. 37

Gulati T, Ramanathan DS, Wong CC, Ganguly K (2014) Reactivation of emergent task-related ensembles during slow-wave sleep after neuroprosthetic learning. *Nature neuroscience* 17:1107–1113. 31

Harris KD (2005) Neural signatures of cell assembly organization. *Nature reviews neuroscience* 6:399–407. 31

Harris KD, Csicsvari J, Hirase H, Dragoi G, Buzsáki G (2003) Organization of cell assemblies in the hippocampus. *Nature* 424:552–556. 4

Hasenstaub A, Sachdev RN, McCormick DA (2007) State changes rapidly modulate cortical neuronal responsiveness. *Journal of Neuroscience* 27:9607–9622. 14, 15

Hatsopoulos NG, Ojakangas CL, Paninski L, Donoghue JP (1998) Information about movement direction obtained from synchronous activity of motor cortical neurons. *Proceedings of the National Academy of Sciences* 95:15706–15711. 20

Hay YA, Deperrois N, Fuchsberger T, Quarrell TM, Koerling AL, Paulsen O (2021) Thalamus mediates neocortical down state transition via gabab-receptor-targeting interneurons. *Neuron* 109:2682–2690. 44

Hebb DO (1949) *The organization of behavior* Wiley. 4, 17

Homma NY, Hullett PW, Atencio CA, Schreiner CE (2020) Auditory Cortical Plasticity Dependent on Environmental Noise Statistics. *Cell Reports* 30:4445–4458.e5. 55

Hu H, Gan J, Jonas P (2014) Fast-spiking, parvalbumin+ gabaergic interneurons: From cellular design to microcircuit function. *Science* 345:1255263. 37

Huang CL, Winer JA (2000) Auditory thalamocortical projections in the cat: laminar and areal patterns of input. *Journal of Comparative Neurology* 427:302–331. 44

Imaizumi K, Priebe NJ, Crum PA, Bedenbaugh PH, Cheung SW, Schreiner CE (2004) Modular functional organization of cat anterior auditory field. *Journal of neurophysiology* 92:444–457. 16

Ince RA, Panzeri S, Kayser C (2013) Neural codes formed by small and temporally precise populations in auditory cortex. *Journal of Neuroscience* 33:18277–18287. 5

Jacobs NS, Chen-Bee CH, Frostig RD (2015) Emergence of spatiotemporal invariance in large neuronal ensembles in rat barrel cortex. *Frontiers in neural circuits* 9:34. 31

Jermakowicz WJ, Chen X, Khaytin I, Bonds A, Casagrande VA (2009) Relationship between spontaneous and evoked spike-time correlations in primate visual cortex. *Journal of neurophysiology* 101:2279–2289. 10, 20

Johnston K, DeSouza JF, Everling S (2009) Monkey prefrontal cortical pyramidal and putative interneurons exhibit differential patterns of activity between prosaccade and antisaccade tasks. *Journal of Neuroscience* 29:5516–5524. 37

Kiani R, Cueva CJ, Reppas JB, Newsome WT (2014) Dynamics of neural population responses in prefrontal cortex indicate changes of mind on single trials. *Current Biology* 24:1542–1547. 31

König P, Engel AK, Singer W (1996) Integrator or coincidence detector? the role of the cortical neuron revisited. *Trends in neurosciences* 19:130–137. 34

Konorski J (1948) *Conditioned reflexes and neuron organization.* Cambridge University Press. 4

Kreiter AK, Singer W (1996) Stimulus-dependent synchronization of neuronal responses in the visual cortex of the awake macaque monkey. *Journal of neuroscience* 16:2381–2396. 5

Kumar A, Rotter S, Aertsen A (2010) Spiking activity propagation in neuronal networks: reconciling different perspectives on neural coding. *Nature reviews neuroscience* 11:615–627. 34

Lankarany M, Al-Basha D, Ratté S, Prescott SA (2019) Differentially synchronized spiking enables multiplexed neural coding. *Proceedings of the National Academy of Sciences* 116:10097–10102. 1, 12, 17, 18, 20, 31

Laubach M, Wessberg J, Nicolelis MA (2000) Cortical ensemble activity increasingly predicts behaviour outcomes during learning of a motor task. *Nature* 405:567–571. 4, 42

Léger JF, Stern EA, Aertsen A, Heck D (2005) Synaptic integration in rat frontal cortex shaped by network activity. *Journal of neurophysiology* 93:281–293. 34, 57

Lewicki MS (2002) Efficient coding of natural sounds. *Nature neuroscience* 5:356–363. 19

Lopes-dos Santos V, Conde-Ocazionez S, Nicolelis MA, Ribeiro ST, Tort AB (2011) Neuronal assembly detection and cell membership specification by principal component analysis. *PLoS ONE* 6. 35

Lopes-dos Santos V, Ribeiro S, Tort AB (2013) Detecting cell assemblies in large neuronal populations. *Journal of Neuroscience Methods* 220:149–166. 1, 7, 57

Luczak A, Barthó P, Harris KD (2009) Spontaneous events outline the realm of possible sensory responses in neocortical populations. *Neuron* 62:413–425. 10, 19

Madar AD, Ewell LA, Jones MV (2019) Temporal pattern separation in hippocampal neurons through multiplexed neural codes. *PLoS computational biology* 15:e1006932. 40

Marčenko VA, Pastur LA (1967) Distribution of Eigenvalues for Some Sets of Random Matrices. *Mathematics of the USSR-Sbornik* 1:457–483. 58

Markram H, Toledo-Rodriguez M, Wang Y, Gupta A, Silberberg G, Wu C (2004) Interneurons of the neocortical inhibitory system. *Nature reviews neuroscience* 5:793–807. 37

McCLURKIN JW, Optican LM (1996) Primate striate and prestriate cortical neurons during discrimination. i. simultaneous temporal encoding of information about color and pattern. *Journal of Neurophysiology* 75:481–495. 40

McCormick DA, Connors BW, Lighthall JW, Prince DA (1985) Comparative electrophysiology of pyramidal and sparsely spiny stellate neurons of the neocortex. *Journal of neurophysiology* 54:782–806. 37

Merzenich MM, Knight PL, Roth GL (1975) Representation of cochlea within primary auditory cortex in the cat. *Journal of Neurophysiology* 38:231–249 PMID: 1092814. 13

Metherate R, Ashe JH (1993) Nucleus basalis stimulation facilitates thalamocortical synaptic transmission in the rat auditory cortex. *Synapse* 14:132–143. 15

Miller JeK, Ayzenshtat I, Carrillo-Reid L, Yuste R (2014) Visual stimuli recruit intrinsically generated cortical ensembles. *Proceedings of the National Academy of Sciences* 111:E4053–E4061. 18

Miller LM, Escabı MA, Read HL, Schreiner CE (2001) Functional convergence of response properties in the auditory thalamocortical system. *Neuron* 32:151–160. 17, 31, 33, 34, 44

Miller LM, Escabí MA, Read HL, Schreiner CE (2002) Spectrotemporal receptive fields in the lemniscal auditory thalamus and cortex. *Journal of Neurophysiology* 87:516–527. 5, 17, 44, 61

Miller LM, Recanzone GH (2009) Populations of auditory cortical neurons can accurately encode acoustic space across stimulus intensity. *Proceedings of the National Academy of Sciences* 106:5931–5935. 5

Miller LM, Schreiner CE (2000) Stimulus-based state control in the thalamocortical system. *Journal of Neuroscience* 20:7011–7016. 57

Mochol G, Hermoso-Mendizabal A, Sakata S, Harris KD, De La Rocha J (2015) Stochastic transitions into silence cause noise correlations in cortical circuits. *Proceedings of the National Academy of Sciences of the United States of America* 112:3529–3534. 63

Mogensen H, Norrlid J, Enander JM, Wahlbom A, Jörntell H (2019) Absence of repetitive correlation patterns between pairs of adjacent neocortical neurons in vivo. *Frontiers in Neural Circuits* 13:1–11. 6

Montijn JS, Meijer GT, Lansink CS, Pennartz CM (2016) Population-level neural codes are robust to single-neuron variability from a multidimensional coding perspective. *Cell reports* 16:2486–2498. 31

Morel A, Rouiller E, de Ribaupierre Y, de Ribaupierre F (1987) Tonotopic organization in the medial geniculate body (MGB) of lightly anesthetized cats. *Experimental Brain Research* 69:24–42. 56

Mountcastle VB (1997) The columnar organization of the neocortex. *Brain: a journal of neurology* 120:701–722. 17

Neske GT (2016) The slow oscillation in cortical and thalamic networks: mechanisms and functions. *Frontiers in neural circuits* 9:88. 14

Niessing J, Friedrich RW (2010) Olfactory pattern classification by discrete neuronal network states. *Nature* 465:47–52. 16

Noback CR (1985) Cerebral cortex. volume 1: Cellular components of the cerebral cortex. 37

Nowak LG, Azouz R, Sanchez-Vives MV, Gray CM, McCormick DA (2003) Electrophysiological classes of cat primary visual cortical neurons in vivo as revealed by quantitative analyses. *Journal of neurophysiology* 89:1541–1566. 37

Oberto VJ, Boucly CJ, Gao H, Todorova R, Zugaro MB, Wiener SI (2022) Distributed cell assemblies spanning prefrontal cortex and striatum. *Current Biology* pp. 1–13. 4, 21, 42, 44, 58, 59

O'Connor DH, Peron SP, Huber D, Svoboda K (2010) Neural activity in barrel cortex underlying vibrissa-based object localization in mice. *Neuron* 67:1048–1061. 19

Pachitariu M, Lyamzin DR, Sahani M, Lesica NA (2015) State-dependent population coding in primary auditory cortex. *Journal of Neuroscience* 35:2058–2073. 21

Pachitariu M, Sridhar S, Stringer C (2023) Solving the spike sorting problem with Kilosort. *bioRxiv* p. 2023.01.07.523036. 56

Paninski L, Shoham S, Fellows MR, Hatsopoulos NG, Donoghue JP (2004) Superlinear population encoding of dynamic hand trajectory in primary motor cortex. *Journal of Neuroscience* 24:8551–8561. 7

Perkel DH, Gerstein GL, Moore GP (1967) Neuronal spike trains and stochastic point processes: Ii. simultaneous spike trains. *Biophysical journal* 7:419–440. 63

Peyrache A, Benchenane K, Khamassi M, Wiener SI, Battaglia FP (2010) Principal component analysis of ensemble recordings reveals cell assemblies at high temporal resolution. *Journal of Computational Neuroscience* 29:309–325. 7

Polley DB, Read HL, Storace DA, Merzenich MM (2007) Multiparametric auditory receptive field organization across five cortical fields in the albino rat. *Journal of Neurophysiology* 97:3621–3638. 55

Qiu A, Schreiner CE, Escabí MA (2003) Gabor analysis of auditory midbrain receptive fields: spectro-temporal and binaural composition. *Journal of neurophysiology* 90:456–476. 61

Read HL, Nauen DW, Escabí MA, Miller LM, Schreiner CE, Winer JA (2011) Distinct core thalamocortical pathways to central and dorsal primary auditory cortex. *Hearing research* 274:95–104. 17

Rosen S (1992) Temporal information in speech: acoustic, auditory and linguistic aspects. *Philosophical Transactions of the Royal Society of London. Series B: Biological Sciences* 336:367–373. 18

Roy SA, Alloway KD (2001) Coincidence detection or temporal integration? what the neurons in somatosensory cortex are doing. *Journal of Neuroscience* 21:2462–2473. 32, 34

Salinas E, Sejnowski TJ (2001) Correlated neuronal activity and the flow of neural information. *Nature reviews neuroscience* 2:539–550. 34

Sanchez-Vives MV, McCormick DA (2000) Cellular and network mechanisms of rhythmic recurrent activity in neocortex. *Nature neuroscience* 3:1027–1034. 14, 15

See JZ, Atencio CA, Sohal VS, Schreiner CE (2018) Coordinated neuronal ensembles in primary auditory cortical columns. *eLife* 7:1–33. 1, 4, 5, 6, 7, 10, 12, 13, 17, 31, 35, 36, 54, 55, 57, 58, 61, 62

See JZ, Homma NY, Atencio CA, Sohal VS, Schreiner CE (2021) Information diversity in individual auditory cortical neurons is associated with functionally distinct coordinated neuronal ensembles. *Scientific Reports* 11:4064. 4, 5, 12, 13, 20, 31, 36, 40, 45

Senzai Y, Fernandez-Ruiz A, Buzsáki G (2019) Layer-specific physiological features and interlaminar interactions in the primary visual cortex of the mouse. *Neuron* 101:500–513. 63

Shahidi N, Andrei AR, Hu M, Dragoi V (2019) High-order coordination of cortical spiking activity modulates perceptual accuracy. *Nature neuroscience* 22:1148–1158. 1, 4, 18

Smith PH, Uhlrich DJ, Manning KA, Banks MI (2012) Thalamocortical projections to rat auditory cortex from the ventral and dorsal divisions of the medial geniculate nucleus. *Journal of Comparative Neurology* 520:34–51. 5

Steinmetz NA, Aydin C, Lebedeva A, Okun M, Pachitariu M, Bauza M, Beau M, Bhagat J, Böhm C, Broux M, Chen S, Colonell J, Gardner RJ, Karsh B, Kloosterman F, Kostadinov D, Mora-Lopez C, O'Callaghan J, Park J, Putzeys J, Sauerbrei B, van Daal RJ, Vollan AZ, Wang S, Welkenhuysen M, Ye Z, Dudman JT, Dutta B, Hantman AW, Harris KD, Lee AK, Moser EI, O'Keefe J, Renart A, Svoboda K, Häusser M, Haesler S, Carandini M, Harris TD (2021) Neuropixels 2.0: A miniaturized high-density probe for stable, long-term brain recordings. *Science* 372. 56

Steriade M, Contreras D, Dossi RC, Nunez A (1993) The slow (¡ 1 hz) oscillation in reticular thalamic and thalamocortical neurons: scenario of sleep rhythm generation in interacting thalamic and neocortical networks. *Journal of Neuroscience* 13:3284–3299. 14, 15

Stevens CF, Zador AM (1998) Input synchrony and the irregular firing of cortical neurons. *Nature neuroscience* 1:210–217. 20

Sukman LJ, Stark E (2022) Cortical pyramidal and parvalbumin cells exhibit distinct spatiotemporal extracellular electric potentials. *Eneuro* 9. 44

Swadlow HA, Gusev AG (2001) The impact of 'bursting' thalamic impulses at a neocortical synapse. *Nature neuroscience* 4:402–408. 32, 36

Tanaka K (1983) Cross-correlation analysis of geniculostriate neuronal relationships in cats. *Journal of neurophysiology* 49:1303–1318. 33

Theunissen FE, Sen K, Doupe AJ (2000) Spectral-temporal receptive fields of nonlinear auditory neurons obtained using natural sounds. *Journal of Neuroscience* 20:2315–2331. 60

Tremblay S, Pieper F, Sachs A, Martinez-Trujillo J (2015) Attentional filtering of visual information by neuronal ensembles in the primate lateral prefrontal cortex. *Neuron* 85:202–215. 18

Tsunada J, Lee JH, Cohen YE (2012) Differential representation of auditory categories between cell classes in primate auditory cortex. *The Journal of physiology* 590:3129–3139. 37

Usrey WM, Alonso JM, Reid RC (2000) Synaptic interactions between thalamic inputs to simple cells in cat visual cortex. *Journal of Neuroscience* 20:5461–5467. 2, 36

Wahlbom A, Mogensen H, Jörntell H (2021) Widely Different Correlation Patterns Between Pairs of Adjacent Thalamic Neurons In vivo. *Frontiers in Neural Circuits* 15:1–10. 6

Walker KM, Bizley JK, King AJ, Schnupp JW (2011) Multiplexed and robust representations of sound features in auditory cortex. *Journal of Neuroscience* 31:14565–14576. 20

Wills TJ, Lever C, Cacucci F, Burgess N, O'Keefe J (2005) Attractor dynamics in the hippocampal representation of the local environment. *Science* 308:873–876. 16

Winer JA (2010) Neurochemical organization of the medial geniculate body and auditory cortex In *The auditory cortex*, pp. 209–234. Springer. 18

Winer JA, Miller LM, Lee CC, Schreiner CE (2005) Auditory thalamocortical transformation: structure and function. *Trends in neurosciences* 28:255–263. 5

Yoshida T, Ohki K (2020)   Natural images are reliably represented by sparse and variable populations of neurons in visual cortex. *Nature communications* 11:872. 4

Yuste R (2015)   From the neuron doctrine to neural networks.   *Nature reviews neuroscience* 16:487–497. 4, 31

Zandvakili A, Kohn A (2015)   Coordinated neuronal activity enhances corticocortical communication. *Neuron* 87:827–839. 2, 4, 20

Zohary E, Shadlen MN, Newsome WT (1994)   Correlated neuronal discharge rate and its implications for psychophysical performance. *Nature* 370:140–143. 20

Zuo Y, Safaai H, Notaro G, Mazzoni A, Panzeri S, Diamond ME (2015)   Complementary contributions of spike timing and spike rate to perceptual decisions in rat s1 and s2 cortex. *Current Biology* 25:357–363. 40

Publishing Agreement

It is the policy of the University to encourage open access and broad distribution of all theses, dissertations, and manuscripts. The Graduate Division will facilitate the distribution of UCSF theses, dissertations, and manuscripts to the UCSF Library for open access and distribution. UCSF will make such theses, dissertations, and manuscripts accessible to the public and will take reasonable steps to preserve these works in perpetuity.

I hereby grant the non-exclusive, perpetual right to The Regents of the University of California to reproduce, publicly display, distribute, preserve, and publish copies of my thesis, dissertation, or manuscript in any form or media, now existing or later derived, including access online for teaching, research, and public service purposes.

DocuSigned by:

Congcong Hu

41991166A991435...   Author Signature

10/30/2023

Date